essential to have a more detailed understanding of the mechanism of neprilysin activation and to identify a regulator of neprilysin activity.

In this report, we show that neurotrophic factors reduce cell surface neprilysin activity (Fig. 1 and supplemental Fig. S1) through regulation of cell surface neprilysin localization (Fig. 4) and that the reduction of neprilysin activity leads to increased Aβ levels (Fig. 3). On the other hand, previous extensive studies have shown that neurotrophic factors, particularly BDNF, exhibit neuroprotective properties that contribute to neuronal survival and memory formation in both rodent and primate models of AD through amyloid-independent mechanisms (40). In addition, BDNF also supports neural stem cells, which have been demonstrated to improve cognition in a transgenic model of AD (41). Furthermore, oligomeric Aβ has been shown to decrease cortical BDNF levels and synaptic function in an AD model mouse (42, 43). These findings together indicate that BDNF would be a useful adjunct in AD therapy to compensate for decreased levels of this neurotrophic factor in the brain and to ameliorate symptoms in the late stages of disease, whereas a strategy involving neprilysin activation could be effective in preventing or delaying the onset of AD because the facilitation of Aβ clearance would attenuate synaptic dysfunction and the reduction in BDNF levels. In fact, with accumulating knowledge, it appears that any treatment for AD is likely to be directed at several targets simultaneously. Our data show that a strategy involving any neurotrophic factor would have as a side effect increased Aβ levels that would have to be taken into account.

The use of neurotrophic factors in this study enabled us to unravel some of the mechanisms controlling neprilysin activity. We found that cell surface neprilysin activity is regulated through the localization of neprilysin to the cell surface, a process that in turn is mediated by phosphorylation/dephosphorylation of the NEP-ICD (Figs. 4 and 5). The regulation of neprilysin activity also involved MEK/ERK signaling, which resulted in phosphorylation of Ser-6 in the NEP-ICD (Figs. 2 and 5), although it remains unclear whether ERK directly phosphorylates the NEP-ICD. Interestingly, casein kinase 2 has been reported to act as a kinase for S6-NEP-ICD phosphorylation (44). Moreover, increased phosphorylation of neprilysin appeared after 24 h of stimulation, indicating that the expression of additional unknown factors might be required.

Although the mechanism remains unclear, metabolism of neprilysin itself would also influence its cell surface activity. Interestingly, T25A-NEP mutant protein could not be detected in transfected cells, despite the presence of the mRNA (supplemental Fig. S5). Speculatively, dephosphorylation of Thr-25 might induce degradation of neprilysin in the cells, as part of a quality control mechanism in the metabolic pathway of neprilysin, although Thr-25 was found to be dephosphorylated in neprilysin located at the cell surface (Fig. 5*D*). Alternatively, the introduced mutation could destabilize the protein and induce aggregation, although the S6A/T25A double mutant was normally expressed in the transfectants (data not shown).

The addition of the PP1a inhibitor tautomycetin to primary cortical/hippocampal neurons extensively increased the phosphorylation state of the NEP-ICD (Fig. 6, *A* and *B*) and reduced cell surface neprilysin activity (Fig. 6*C*). A closer examination of the NEP-ICD amino acid sequence revealed a peptide sequence, KKKQRW, similar to the PP1a binding motif, suggesting that the NEP-ICD might be a target of PP1a. Indeed, PP1a was found to be associated with neprilysin in SH-SY5Y cell extracts, and overexpression of PP1a stimulated cell surface neprilysin activity, leading to reduced Aβ levels (Fig. 6, *D–G*). Therefore, activation of PP1a (*e.g.* pharmacologically) would be a possible strategy to increase cell surface neprilysin activity. Interestingly, it has been reported that PP1a activity was regulated by DARPP32, an endogenous regulator of PP1a (45), and that DARPP32 levels are reduced in the brains of somatostatin receptor-1 (SSTR1) and SSTR5 double knock-out mice (46). These observations, considered together with our previous data showing that presynaptic localization of neprilysin is significantly decreased in the hippocampus of somatostatin-deficient mice (18), indicate that somatostatin possibly regulates neprilysin activity through PP1 activity. Thus, SSTR agonists might be successful drug candidates for the treatment of AD.

With the development of new gene therapy technologies, application of a neprilysin gene transfer strategy could be a potential way to decrease Aβ levels and delay the onset of amyloidosis. Considering the increased activity of S6-NEP, an alternative would be to introduce the S6A-NEP mutant, possibly leading to even more efficient Aβ degradation compared with that of WT-NEP.

In conclusion, our results show that the phosphorylation state of the intracellular domain regulates cell surface neprilysin activity and extracellular Aβ levels due to the modulation of neprilysin localization. We propose that enhancing cell surface neprilysin activity, for example by maintaining S6 of the NEP-ICD in a dephosphorylated state, either through activation of phosphatases or through inhibition of the kinase responsible for phosphorylation at the S6-NEP-ICD, would be beneficial for the prevention of Aβ amyloidosis.

Acknowledgment—We thank Dr. C. Gerard for providing neprilysin-deficient mice.

REFERENCES

1. Hardy, J., and Selkoe, D. J. (2002) The amyloid hypothesis of Alzheimer's disease. Progress and problems on the road to therapeutics. *Science* **297,** 353–356
2. Selkoe, D. J. (1994) Alzheimer's disease. A central role for amyloid. *J. Neuropathol. Exp. Neurol.* **53,** 438–447
3. Selkoe, D. J. (1994) Cell biology of the amyloid β-protein precursor and the mechanism of Alzheimer's disease. *Annu. Rev. Cell Biol.* **10,** 373–403
4. Saito, T., Suemoto, T., Brouwers, N., Sleegers, K., Funamoto, S., Mihira, N., Matsuba, Y., Yamada, K., Nilsson, P., Takano, J., Nishimura, M., Iwata, N., Van Broeckhoven, C., Ihara, Y., and Saido, T. C. (2011) Potent amyloidogenicity and pathogenicity of Aβ43. *Nat. Neurosci.* **14,** 1023–1032
5. Saido, T. C. (1998) Alzheimer's disease as proteolytic disorders. Anabolism and catabolism of β-amyloid. *Neurobiol. Aging* **19,** S69–S75
6. Iwata, N., Tsubuki, S., Takaki, Y., Shirotani, K., Lu, B., Gerard, N. P., Gerard, C., Hama, E., Lee, H. J., and Saido, T. C. (2001) Metabolic regulation of brain Aβ by neprilysin. *Science* **292,** 1550–1552
7. Iwata, N., Tsubuki, S., Takaki, Y., Watanabe, K., Sekiguchi, M., Hosoki, E., Kawashima-Morishima, M., Lee, H. J., Hama, E., Sekine-Aizawa, Y., and Saido, T. C. (2000) Identification of the major Aβ1–42-degrading catabolic pathway in brain parenchyma. suppression leads to biochemical and pathological deposition. *Nat. Med.* **6,** 143–150

8. Caccamo, A., Oddo, S., Sugarman, M. C., Akbari, Y., and LaFerla, F. M. (2005) Age- and region-dependent alterations in Aβ-degrading enzymes. implications for Aβ-induced disorders. *Neurobiol. Aging* **26,** 645–654
9. Reilly, C. E. (2001) Neprilysin content is reduced in Alzheimer brain areas. *J. Neurol.* **248,** 159–160
10. Carter, T. L., Pedrini, S., Ghiso, J., Ehrlich, M. E., and Gandy, S. (2006) Brain neprilysin activity and susceptibility to transgene-induced Alzheimer amyloidosis. *Neurosci. Lett.* **392,** 235–239
11. Iwata, N., Takaki, Y., Fukami, S., Tsubuki, S., and Saido, T. C. (2002) Region-specific reduction of Aβ-degrading endopeptidase, neprilysin, in mouse hippocampus upon aging. *J. Neurosci. Res.* **70,** 493–500
12. Yasojima, K., Akiyama, H., McGeer, E. G., and McGeer, P. L. (2001) Reduced neprilysin in high plaque areas of Alzheimer brain. A possible relationship to deficient degradation of β-amyloid peptide. *Neurosci. Lett.* **297,** 97–100
13. Huang, S. M., Mouri, A., Kokubo, H., Nakajima, R., Suemoto, T., Higuchi, M., Staufenbiel, M., Noda, Y., Yamaguchi, H., Nabeshima, T., Saido, T. C., and Iwata, N. (2006) Neprilysin-sensitive synapse-associated amyloid-β peptide oligomers impair neuronal plasticity and cognitive function. *J. Biol. Chem.* **281,** 17941–17951
14. Farris, W., Schütz, S. G., Cirrito, J. R., Shankar, G. M., Sun, X., George, A., Leissring, M. A., Walsh, D. M., Qiu, W. Q., Holtzman, D. M., and Selkoe, D. J. (2007) Loss of neprilysin function promotes amyloid plaque formation and causes cerebral amyloid angiopathy. *Am. J. Pathol.* **171,** 241–251
15. Iwata, N., Mizukami, H., Shirotani, K., Takaki, Y., Muramatsu, S., Lu, B., Gerard, N. P., Gerard, C., Ozawa, K., and Saido, T. C. (2004) Presynaptic localization of neprilysin contributes to efficient clearance of amyloid-β peptide in mouse brain. *J. Neurosci.* **24,** 991–998
16. El-Amouri, S. S., Zhu, H., Yu, J., Marr, R., Verma, I. M., and Kindy, M. S. (2008) Neprilysin. An enzyme candidate to slow the progression of Alzheimer's disease. *Am. J. Pathol.* **172,** 1342–1354
17. Leissring, M. A., Farris, W., Chang, A. Y., Walsh, D. M., Wu, X., Sun, X., Frosch, M. P., and Selkoe, D. J. (2003) Enhanced proteolysis of β-amyloid in APP transgenic mice prevents plaque formation, secondary pathology, and premature death. *Neuron* **40,** 1087–1093
18. Saito, T., Iwata, N., Tsubuki, S., Takaki, Y., Takano, J., Huang, S. M., Suemoto, T., Higuchi, M., and Saido, T. C. (2005) Somatostatin regulates brain amyloid β peptide Aβ42 through modulation of proteolytic degradation. *Nat. Med.* **11,** 434–439
19. Saido, T. C., Nagao, S., Shiramine, M., Tsukaguchi, M., Sorimachi, H., Murofushi, H., Tsuchiya, T., Ito, H., and Suzuki, K. (1992) Autolytic transition of μ-calpain upon activation as resolved by antibodies distinguishing between the pre- and post-autolysis forms. *J. Biochem.* **111,** 81–86
20. Saido, T. C., Iwatsubo, T., Mann, D. M., Shimada, H., Ihara, Y., and Kawashima, S. (1995) Dominant and differential deposition of distinct beta-amyloid peptide species, Aβ N3(pE), in senile plaques. *Neuron* **14,** 457–466
21. Pagans, S., Sakane, N., Schnölzer, M., and Ott, M. (2011) Characterization of HIV Tat modifications using novel methyl-lysine-specific antibodies. *Methods* **53,** 91–96
22. Hussain, I., Hawkins, J., Harrison, D., Hille, C., Wayne, G., Cutler, L., Buck, T., Walter, D., Demont, E., Howes, C., Naylor, A., Jeffrey, P., Gonzalez, M. I., Dingwall, C., Michel, A., Redshaw, S., and Davis, J. B. (2007) Oral administration of a potent and selective non-peptidic BACE-1 inhibitor decreases β-cleavage of amyloid precursor protein and amyloid-β production *in vivo*. *J. Neurochem.* **100,** 802–809
23. Shirotani, K., Tsubuki, S., Iwata, N., Takaki, Y., Harigaya, W., Maruyama, K., Kiryu-Seo, S., Kiyama, H., Iwata, H., Tomita, T., Iwatsubo, T., and Saido, T. C. (2001) Neprilysin degrades both amyloid β peptides 1–40 and 1–42 most rapidly and efficiently among thiorphan- and phosphoramidon-sensitive endopeptidases. *J. Biol. Chem.* **276,** 21895–21901
24. Berndt, N., Dohadwala, M., and Liu, C. W. (1997) Constitutively active protein phosphatase 1α causes Rb-dependent G_1 arrest in human cancer cells. *Curr. Biol.* **7,** 375–386
25. Hama, E., Shirotani, K., Iwata, N., and Saido, T. C. (2004) Effects of neprilysin chimeric proteins targeted to subcellular compartments on amyloid β peptide clearance in primary neurons. *J. Biol. Chem.* **279,** 30259–30264
26. Takaki, Y., Iwata, N., Tsubuki, S., Taniguchi, S., Toyoshima, S., Lu, B., Gerard, N. P., Gerard, C., Lee, H. J., Shirotani, K., and Saido, T. C. (2000) Biochemical identification of the neutral endopeptidase family member responsible for the catabolism of amyloid β peptide in the brain. *J. Biochem.* **128,** 897–902
27. Rappoport, J. Z., and Simon, S. M. (2003) Real-time analysis of clathrin-mediated endocytosis during cell migration. *J. Cell Sci.* **116,** 847–855
28. Barbacid, M. (1994) The Trk family of neurotrophin receptors. *J. Neurobiol.* **25,** 1386–1403
29. Segal, R. A., and Greenberg, M. E. (1996) Intracellular signaling pathways activated by neurotrophic factors. *Annu. Rev. Neurosci.* **19,** 463–489
30. Segal, R. A. (2003) Selectivity in neurotrophin signaling. Theme and variations. *Annu. Rev. Neurosci.* **26,** 299–330
31. Loeb, D. M., Tsao, H., Cobb, M. H., and Greene, L. A. (1992) NGF and other growth factors induce an association between ERK1 and the NGF receptor, gp140prototrk. *Neuron* **9,** 1053–1065
32. Zheng, H., and Koo, E. H. (2006) The amyloid precursor protein. Beyond amyloid. *Mol. Neurodegener.* **1,** 5
33. Eckman, E. A., Watson, M., Marlow, L., Sambamurti, K., and Eckman, C. B. (2003) Alzheimer's disease β-amyloid peptide is increased in mice deficient in endothelin-converting enzyme. *J. Biol. Chem.* **278,** 2081–2084
34. Farris, W., Mansourian, S., Chang, Y., Lindsley, L., Eckman, E. A., Frosch, M. P., Eckman, C. B., Tanzi, R. E., Selkoe, D. J., and Guenette, S. (2003) Insulin-degrading enzyme regulates the levels of insulin, amyloid β-protein, and the β-amyloid precursor protein intracellular domain *in vivo*. *Proc. Natl. Acad. Sci. U.S.A.* **100,** 4162–4167
35. Pawson, T., and Scott, J. D. (1997) Signaling through scaffold, anchoring, and adaptor proteins. *Science* **278,** 2075–2080
36. Sumitomo, M., Iwase, A., Zheng, R., Navarro, D., Kaminetzky, D., Shen, R., Georgescu, M. M., and Nanus, D. M. (2004) Synergy in tumor suppression by direct interaction of neutral endopeptidase with PTEN. *Cancer Cell* **5,** 67–78
37. Roy, J., and Cyert, M. S. (2009) Cracking the phosphatase code. Docking interactions determine substrate specificity. *Sci. Signal.* **2,** re9
38. Hurley, T. D., Yang, J., Zhang, L., Goodwin, K. D., Zou, Q., Cortese, M., Dunker, A. K., and DePaoli-Roach, A. A. (2007) Structural basis for regulation of protein phosphatase 1 by inhibitor-2. *J. Biol. Chem.* **282,** 28874–28883
39. Iwata, N., Higuchi, M., and Saido, T. C. (2005) Metabolism of amyloid-beta peptide and Alzheimer's disease. *Pharmacol. Ther.* **108,** 129–148
40. Nagahara, A. H., Merrill, D. A., Coppola, G., Tsukada, S., Schroeder, B. E., Shaked, G. M., Wang, L., Blesch, A., Kim, A., Conner, J. M., Rockenstein, E., Chao, M. V., Koo, E. H., Geschwind, D., Masliah, E., Chiba, A. A., and Tuszynski, M. H. (2009) Neuroprotective effects of brain-derived neurotrophic factor in rodent and primate models of Alzheimer's disease. *Nat. Med.* **15,** 331–337
41. Blurton-Jones, M., Kitazawa, M., Martinez-Coria, H., Castello, N. A., Müller, F. J., Loring, J. F., Yamasaki, T. R., Poon, W. W., Green, K. N., and LaFerla, F. M. (2009) Neural stem cells improve cognition via BDNF in a transgenic model of Alzheimer disease. *Proc. Natl. Acad. Sci. U.S.A.* **106,** 13594–13599
42. Peng, S., Garzon, D. J., Marchese, M., Klein, W., Ginsberg, S. D., Francis, B. M., Mount, H. T., Mufson, E. J., Salehi, A., and Fahnestock, M. (2009) Decreased brain-derived neurotrophic factor depends on amyloid aggregation state in transgenic mouse models of Alzheimer's disease. *J. Neurosci.* **29,** 9321–9329
43. Zheng, Z., Sabirzhanov, B., and Keifer, J. (2010) Oligomeric amyloid-β inhibits the proteolytic conversion of brain-derived neurotrophic factor (BDNF), AMPA receptor trafficking, and classical conditioning. *J. Biol. Chem.* **285,** 34708–34717
44. Siepmann, M., Kumar, S., Mayer, G., and Walter, J. (2010) Casein kinase 2 dependent phosphorylation of neprilysin regulates receptor tyrosine kinase signaling to Akt. *PLoS One* **5,** e13134
45. Greengard, P., Allen, P. B., and Nairn, A. C. (1999) Beyond the dopamine receptor. The DARPP-32/protein phosphatase-1 cascade. *Neuron* **23,** 435–447
46. Rajput, P. S., Kharmate, G., Norman, M., Liu, S. H., Sastry, B. R., Brunicardi, C. F., and Kumar, U. (2011) Somatostatin receptor 1 and 5 double knockout mice mimic neurochemical changes of Huntington's disease transgenic mice. *PLoS One* **6,** e24467

Neurobiology of Disease

Transgenic Expression of Intraneuronal $A\beta_{42}$ But Not $A\beta_{40}$ Leads to Cellular $A\beta$ Lesions, Degeneration, and Functional Impairment without Typical Alzheimer's Disease Pathology

Dorothee Abramowski,[1]* Sabine Rabe,[1]* Ajeet Rijal Upadhaya,[2] Julia Reichwald,[1] Simone Danner,[1] Dieter Staab,[1] Estibaliz Capetillo-Zarate,[3] Haruyasu Yamaguchi,[4] Takaomi C. Saido,[5] Karl-Heinz Wiederhold,[1] Dietmar Rudolf Thal,[2] and Matthias Staufenbiel[1]

[1]Novartis Institutes for Biomedical Research, CH-4056 Basel, Switzerland, [2]Institute of Pathology–Laboratory of Neuropathology, University of Ulm, 89081 Ulm, Germany, [3]Weill Medical College of Cornell University, New York, New York 10021, [4]Gunma University School of Health Sciences, Gunma 371-8514, Japan, and [5]Laboratory of Proteolytic Neuroscience, RIKEN Brain Science Institute, Saitama 351-0198, Japan

An early role of amyloid-β peptide ($A\beta$) aggregation in Alzheimer's disease pathogenesis is well established. However, the contribution of intracellular or extracellular forms of $A\beta$ to the neurodegenerative process is a subject of considerable debate. We here describe transgenic mice expressing $A\beta_{1-40}$ (APP47) and $A\beta_{1-42}$ (APP48) with a cleaved signal sequence to insert both peptides during synthesis into the endoplasmic reticulum. Although lower in transgene mRNA, APP48 mice reach a higher brain $A\beta$ concentration. The reduced solubility and increased aggregation of $A\beta_{1-42}$ may impair its degradation. APP48 mice develop intracellular $A\beta$ lesions in dendrites and lysosomes. The hippocampal neuron number is reduced already at young age. The brain weight decreases during aging in conjunction with severe white matter atrophy. The mice show a motor impairment. Only very few $A\beta_{1-40}$ lesions are found in APP47 mice. Neither APP47 nor APP48 nor the bigenic mice develop extracellular amyloid plaques. While intracellular membrane expression of $A\beta_{1-42}$ in APP48 mice does not lead to the AD-typical lesions, $A\beta$ aggregates develop within cells accompanied by considerable neurodegeneration.

Introduction

Various lines of evidence point to a central role of the amyloid-β peptide ($A\beta$) in the development of Alzheimer's disease (AD) (for review, see Citron, 2010). Although the disorder is etiologically heterogeneous, aggregation of $A\beta$ appears as an early pathogenic event common to all forms of AD. Aggregated $A\beta$ shows no overt acute toxicity *in vivo* in accordance with the slow progression of this chronic neurodegenerative condition (Jack et al., 2010). In human brain, $A\beta$ deposits may persist for extended periods of time until clinical symptoms become evident. Amyloid plaque-forming β-amyloid precursor protein (APP) transgenic mouse models of AD show correspondingly little neurodegeneration during their life span. $A\beta$ aggregates can affect neuronal processes at multiple levels, which may lead to a slow decompensation of functionally connected networks (Palop and Mucke, 2010). The molecular structure of the pathogenic species remains a matter of considerable debate. Both amyloid plaques, one of the pathological hallmarks of AD, as well as oligomeric forms of $A\beta$ have been implicated as pathogenic (Shankar et al., 2008; Nimmrich and Ebert, 2009). It also remains unclear to what extent intracellular and extracellular $A\beta$ aggregates contribute to pathogenesis (Gouras et al., 2010).

Recently, transgenic mice have been described expressing either of the two major $A\beta$ isoforms, $A\beta_{1-40}$ and $A\beta_{1-42}$, fused to the C terminus of the BRI protein (McGowan et al., 2005). Cleavage of the fusion proteins at a furin site leads to efficient secretion of $A\beta$ peptides. These animals demonstrated that $A\beta_{1-42}$ but not $A\beta_{1-40}$ is sufficient to promote $A\beta$ deposition *in vivo*. Overt toxicity, however, has not been found, suggesting that intracellular species might be responsible. To address this question, we have generated transgenic mice expressing intracellular $A\beta_{1-40}$ and $A\beta_{1-42}$. The peptides are preceded by a cleaved N-terminal signal sequence to cotranslationally insert them into the endoplasmic reticulum. Both transgenic lines do not develop extracellular amyloid plaques, but $A\beta_{42}$ mice (APP48) show intracellular $A\beta$ lesions. Additionally, hippocampal neurons and white matter are reduced along with a motor impairment indicating neurodegeneration in the absence of typical AD pathology.

Materials and Methods

Animal studies. A cDNA fragment encoding the rat preproenkephalin signal peptide (SPENK) was amplified from a rat brain cDNA library and ligated to cDNAs encoding human $A\beta_{1-40}$ or $A\beta_{1-42}$, followed by a TAG stop codon. The resulting SPENK-$A\beta_{40}$ or SPENK-$A\beta_{42}$ cDNA was

Received Sept. 8, 2011; accepted Dec. 2, 2011.

Author contributions: D.A., S.R., J.R., K.-H.W., D.R.T., and M.S. designed research; D.A., S.R., A.R.U., J.R., S.D., D.S., and K.-H.W. performed research; E.C.-Z., H.Y., and T.C.S. contributed unpublished reagents/analytic tools; D.A., S.R., A.R.U., J.R., S.D., D.S., K.-H.W., D.R.T., and M.S. analyzed data; D.R.T. and M.S. wrote the paper.

This work was supported by Deutsche Forschungsgemeinschaft Grant TH624/6-1 and Alzheimer Forschung Initiative Grant 10810 (D.R.T.). We gratefully thank Irina Kosterin, Domenico Ammaturo, and Andre Schade for technical help. We also acknowledge Dr. Laura Jacobson for help with statistical analyses.

The authors declare no competing financial interests.

*D.A. and S.R. contributed equally to this work.

Correspondence should be addressed to Dr. Matthias Staufenbiel, Novartis Pharma AG, Forum 1, Novartis Campus, CH-4056 Basel, Switzerland. E-mail: matthias.staufenbiel@novartis.com.

DOI:10.1523/JNEUROSCI.4586-11.2012

 0270-6474/12/321273-11$15.00/0

cloned into the pTSC21 plasmid for expression under the control of the mouse Thy-1 promoter. The same promoter was used to express APP with the KM670/671NL "Swedish" mutation in APP23 mice as described previously (Sturchler-Pierrat et al., 1997). The mice were on a C57BL/6 background and hemizygous for the transgene. They were killed, and tissues were prepared as described previously (Abramowski et al., 2008). All animal experiments were in compliance with protocols approved by the Swiss Animal Care and Use Committees.

Biochemical assays. Brain samples were processed and analyzed for Aβ peptides [immunoprecipitation of Aβ and Western blotting or matrix-assisted laser desorption ionization time-of-flight (MALDI-TOF), electrochemiluminescence-linked immunoassay (MSD 96-Well Multi-Array Human (6E10) $A\beta_{40}$ or $A\beta_{42}$ Ultra-Sensitive kits; Meso Scale Discovery)] as described previously (Abramowski et al., 2008).

Sequential Aβ extraction and immunoprecipitation. For Triton X-100 (TX-100) (93418; Fluka/Sigma-Aldrich) extraction, forebrain homogenates were extracted with 1% TX-100 in TBS–Complete for 15 min on ice and ultracentrifuged (100,000 × *g*, 4°C, 15 min), and the clear supernatants were immunoprecipitated as described below. The pellets were used for further SDS extraction. Subsequently, TX-100 pellets were extracted with SDS in TBS–Complete for 15 min at room temperature either with 1 or 2% SDS. The extracts with 1% SDS were diluted after extraction to 0.1% final SDS concentration with TBS–Complete. After ultracentrifugation (100,000 × *g*, 4°C, 15 min), immunoprecipitation from the clear supernatant was done with 6E10 and the pellets were used for further formic acid extraction. Extracts with 2% SDS were ultracentrifuged (100,000 × *g*, 20°C, 15 min), and the supernatants were subsequently diluted to a final 0.1% SDS concentration. These SDS extracts and formic acid-extracted pellets were immunoprecipitated with 4G8 (SIG-39200; Covance) only. SDS pellets were extracted with 70% formic acid for 15 min at room temperature, neutralized with 19 vol (v/v) 1 M Tris-base/1% TX-100/Complete and ultracentrifuged (100,000 × *g*, 4°C, 15 min). The clear supernatant was used for immunoprecipitation, and the pellet was discarded. Aβ standards were prepared by spiking synthetic Aβ peptides to nontransgenic forebrain extracts processed the same as described for the samples.

All extracts were either immunoprecipitated with 6E10 (SIG-39300; Covance) bound to Dynabeads Protein G (100.03; Invitrogen) or 4G8 (SIG-39200; Covance) bound to Protein G-Sepharose 4 Fast Flow (17-0618-01; GE Healthcare Life Sciences) and incubated overnight at 4°C on end-over-end rotor. After incubation, the supernatants were removed, and the Dynabeads were washed with TBS–Complete/1% NP-40, then with 10 mM Tris-HCl, pH 7.5, and finally with 1 mM Tris-HCl, pH 7.5. Sepharose beads were washed once with 20 mM Tris-HCl, pH 7.5. Samples were boiled with sample buffer for 5 min at 95°C and analyzed on Western blot.

Sequential immunoprecipitation. For sequential immunoprecipitation, forebrain homogenates were extracted with 1% TX-100 as described above. To the extract, α Aβ (N3pE) antibody (18591; IBL)-bound Dynabeads Protein G were added and incubated overnight at 4°C on end-over-end rotor. After incubation, the supernatants were transferred to fresh tubes and the extracts were immunoprecipitated a second time with 6E10 antibody bound to Dynabeads Protein G as described above. The beads from both immunoprecipitations were processed the same as described above.

Western blot. For Aβ peptide determination on Western blot, forebrain homogenates were separated on a 13% Tris-bicine gel with 8 M urea as described previously (Klafki et al., 1996; Staufenbiel and Paganetti, 2000). In this gel system, the different Aβ peptides are well separated. Proteins were transferred to Immobilon-P membranes (Millipore). Aβ peptides were heat fixed to the membrane by boiling for 3 min in PBS (P4417; Sigma-Aldrich). Aβ peptides were detected with 6E10 (SIG-39300; Covance) or N3pE Aβ with α Aβ (N3pE) antibody (18591; IBL). Proteins were detected by visualizing chemiluminescence (ECL Advance or ECL Plus; GE Healthcare) on autoradiographic films (Hyperfilm ECL; GE Healthcare).

In situ *hybridization.* The spatial distribution pattern of SPENK-$A\beta_{40}$ or SPENK-$A\beta_{42}$ transgene expression was determined by *in situ* hybridization (Sturchler-Pierrat et al., 1997) with a ^{33}P-labeled oligonucleotide (5′-CGCCCACCATGAGTCCAATGATTGCACCTTTGTTTGAACC-3′). The probe binds entirely within the Aβ-coding part. It contains four mismatches compared with the mouse APP sequence and did not cross-react with mouse APP RNA.

RNA quantification. Total RNA extraction, cDNA synthesis, and real-time PCR gene expression analysis and quantification were done as described by Reichwald et al. (2009). TaqMan Gene Expression Assays were ordered from Eurogentec (18s rRNA control kit FAM-TAMRA; RT-CKFT-18s) or designed (SPENK40/42F1: CAG AGG AAG GAC CTC GAA GCT; SPENK40/42R1: AAC AAA GGT GCA ATC ATT GGA CT; MGB Taq40: FAM-TCG ACC TAG ACA ACA CC-MGBNFQ; MGB Taq42: FAM-TCG ACC TAC GCT ATG ACA-MGBNFQ). Real-time PCR quantifications were run in triplicate for each sample and the average determined. Mice were analyzed in groups of 10 per genotype.

Neuropathology and immunocytochemistry. Tissue fixation, sectioning, and processing were done as described previously (Sturchler-Pierrat et al., 1997; Abramowski et al., 2008). Conventional silver staining for axonal neurofilaments was performed with the Bodian method. The Campbell–Switzer silver impregnation was used to stain fibrillar Aβ with high sensitivity (Braak and Braak, 1991; Thal et al., 1999).

Immunohistochemistry was performed for the detection and quantification of Aβ pathology in APP48. Before the use of monoclonal mouse antibodies, 100-μm-thick free-floating sections were incubated with goat anti-mouse IgG for blocking intrinsic mouse IgG (Thal et al., 2007). To detect $A\beta_{1-42}$-positive material, the sections were stained with monoclonal antibodies specifically detecting the C terminus of $A\beta_{42}$ [MBC42 (Yamaguchi et al., 1998); 1/200; formic acid pretreatment; 24 h at 22°C] or with an antibody raised against $A\beta_{17-24}$ (4G8; Covance; 1/5000; formic acid pretreatment; 24 h at 22°C), with an antibody directed against the N terminus of $A\beta_{1-42}$ [AβN1D (Saido et al., 1995); polyclonal rabbit; 1/100; formic acid and microwave pretreatment], and with anti-AβN3pE (polyclonal rabbit; IBL; 1/100; formic acid and microwave pretreatment). To exclude tau and TDP43 pathology, an antibody against abnormal phosphorylated tau protein (AT-8; monoclonal mouse; Thermo Fisher Scientific; 1/1000; 24 h at 22°C) and an antibody against phosphorylated TDP43 (pTDP43: pS409/410-2; Cosmo Bio; 1/10,000; microwave pretreatment) were used. Astrocytes were labeled with an antibody directed against the glial fibrillary acidic protein (GFAP) (polyclonal rabbit; Dako; 1/1000; 24 h at 22°C), microglial cells with *Ricinus communis* agglutinin (RCA) (Vector Laboratories; 1/250; 24 h at 22°C). To test whether APP was present in Aβ aggregates or in plaque-associated dystrophic neurites, antibodies directed against APP were used (22C11; monoclonal mouse; Millipore Bioscience Research Reagents; 1/75; 24 h at 22°C). To identify abnormalities in the neuronal network, sections of each mouse were stained with antibodies against 68 kDa subunits of neurofilament protein (NF-L; SPM 204; Zytomed; 1/100; microwave pretreatment; 24 h at 22°C) and synaptophysin (polyclonal rabbit; Dako; 1/1000; microwave pretreatment). The primary antibodies were detected with a biotinylated secondary antibody and the ABC complex (Biomeda), and visualized with diaminobenzidine-HCl (DAB) (Hsu et al., 1981). Sections were mounted in Eukitt (Kindler). Biotinylated RCA was detected with the ABC complex and visualized with DAB.

For double immunofluorescence, 20-μm-thick free-floating sections were incubated with rabbit Aβ antiserum NT11 and monoclonal antibody (clone AP20; Millipore Bioscience Research Reagents) against microtubule-associated protein 2 (MAP2) as dendritic marker. Alternatively, CD45 monoclonal antibody MCA1031G (Serotec) was used to label microglia cells. Primary antibodies were detected with horseradish peroxidase (HRP)-labeled anti-rabbit IgG (Dako) and HRP-labeled anti-mouse IgG (Dako) secondary antibodies. Signal Amplification has been done by applying Cy3- or FITC-conjugated Tyramide (NEL741; PerkinElmer).

To determine the intracellular location of Aβ-reactive structures, labeling with Aβ antibody 4G8 was colocalized with antibody labeling of different compartmental markers: LAMP-1 (ab62562; Abcam) for late endosomes/lysosomes, EEA1 (ab2900; Abcam) for early endosomes, BiP (anti-KDEL; SPA-827; Stressgen) for post-endoplasmatic reticulum compartments, and TIA-1/TIAR(D-9) (sc-48371; Santa Cruz) for stress granules. Aβ was detected with Cy2-labeled secondary antibodies,

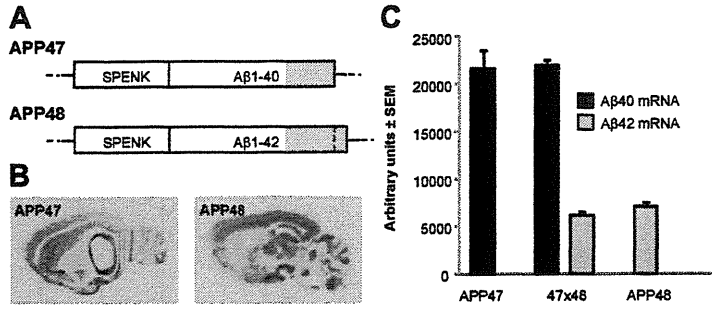

Figure 1. APP47 and APP48 transgenes and brain mRNA expression. ***A***, Schematic representation of the APP47 and APP48 expression constructs. The box represents the translated sequence comprising the cleaved N-terminal signal sequence SPENK (signal peptide preproenkephalin) followed by $A\beta_{1-40}$ or $A\beta_{1-42}$. The gray C-terminal end denotes the hydrophobic amino acid stretch of Aβ, which is approximately one-half of the APP transmembrane region (located in the luminal leaflet of the membrane bilayer). ***B***, *In situ* hybridization to locate the transgene expression in 2-month-old APP47 and APP48 mouse brain. ***C***, Relative transgene mRNA levels in forebrain of female APP47, APP48, and APP47 × APP48 (47 × 48) mice as determined by quantitative PCR. Animals were 2 months of age. Differences between $A\beta_{1-40}$ and $A\beta_{1-42}$ mRNAs were statistically significant (Student's *t* test, two-tailed, $p < 0.0001$), whereas the same mRNAs did not differ significantly ($p > 0.1$) between single- and double-transgenic mice. Error bars indicate SEM.

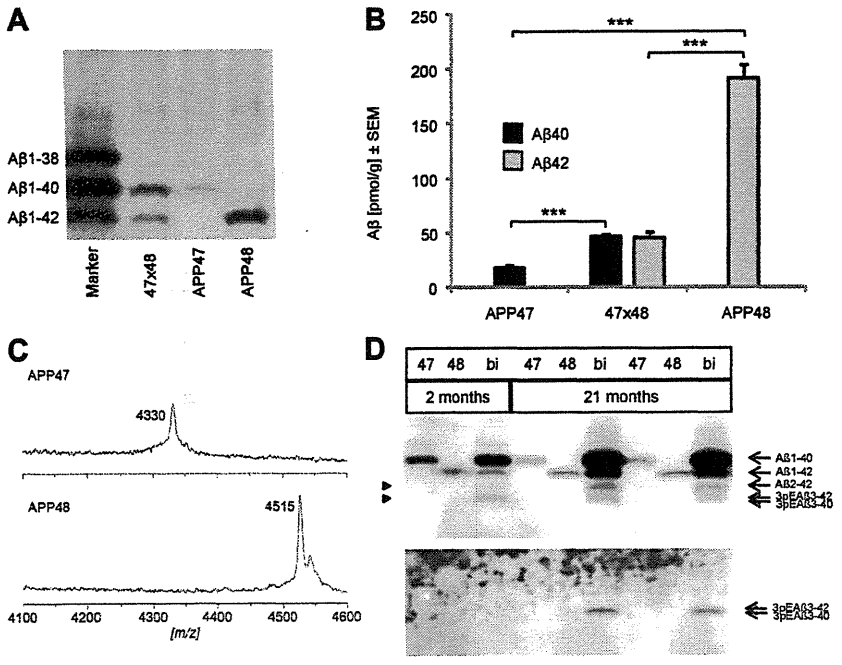

Figure 2. Characterization of human $A\beta_{40}$ and $A\beta_{42}$ peptides in brain. ***A***, Western blot of forebrain homogenates from representative Aβ-expressing mice at 2 months. Female mice are shown, but results were similar for males. Homogenates were dissolved in SDS-sample buffer and run on a SDS/urea gel to separate $A\beta_{1-40}$ and $A\beta_{1-42}$. The gel was overloaded to improve detection. Synthetic Aβ peptides spiked into a nontransgenic mouse brain homogenate are shown on the left. Note that $A\beta_{1-40}$ and $A\beta_{1-42}$ blot with different efficiency and cannot be compared directly. ***B***, Formic acid-extracted total Aβ was quantified by an electrochemoluminescence assay (MSD). Significant differences (Student's *t* test, two-tailed) are indicated by asterisks: ***$p <$ 0.001. One-way ANOVA and Tukey's test showed a significant difference between $A\beta_{40}$ and $A\beta_{42}$ in APP47 versus APP48 mice ($p < 0.001$) but not within the double-transgenic animals (47 × 48; Student's *t* test, two-tailed, $p = 0.83$). Error bars indicate SEM. ***C***, MALDI spectra of immunoprecipitates with Aβ antibody 6E10 from brain extracts of APP47 and APP48 mice showed peaks at the expected molecular weight of $A\beta_{1-40}$ and $A\beta_{1-42}$, respectively. ***D***, Forebrain homogenates of 2- and 21-month-old APP47, APP48, and APP47 × APP48 (47 × 48) mice were immunoprecipitated with Aβ antibody 6E10, separated on a SDS/urea gel, and detected by Western blotting using an N3pE (pyroglutamate; upper panel) or general (6E10; lower panel) Aβ antibody. The two faster migrating bands are indicated by arrowheads. Pyroglutamate Aβ was detected as a minor portion of the fastest band in aged double-transgenic mice only. The migration positions of synthetic standards are indicated on the right.

whereas the compartmental markers were detected with Cy3-labeled secondary antibodies.

In the event that single-label immunohistochemistry was performed on paraffin sections, a counterstaining with hematoxylin was applied. The immunostained sections were analyzed with a Leica DMLB fluorescence microscope (Leica). Quantification of Aβ pathology in APP48 was performed in the area of the frontocentral neocortex.

Stereology. Six APP48 and six wild-type mice, 18 months of age, were used for stereology. One hundred-micrometer-thick coronal sections were stained with the aldehyde fuchsin–Darrow red method exhibiting a Nissl-like staining pattern of the neurons and the pigment architecture for anatomical parcellation (Braak, 1974). The frontocentral cortex volume for stereology was defined as the volume of the subfields M2, M1, S1 starting at the level of the anterior commissure as described previously (Capetillo-Zarate et al., 2006). The CA1 volume was measured in serial 100-μm-thick sections. Quantification of neurons was performed for the frontocentral cortex and the hippocampal sector CA1, separately, according to the principles of unbiased stereology (Schmitz and Hof, 2000).

The number of specific types of Aβ aggregates in the frontocentral neocortex was counted in accordance with the principles of unbiased stereology.

The relative volume of the forebrain white matter was determined by measuring the area of the Luxol fast blue (LFB)-stained forebrain white matter and the total area of the forebrain in the same section. The percentage of the hemispheres covered by white matter was calculated as follows: Forebrain white matter volume (%) = (forebrain area stained with LFB × 100)/total forebrain area.

Electron microscopy and immuno-electron microscopy. One 100-μm-thick vibratome section of the frontocentral cortex of six 18-month-old wild-type and APP48/167 mice was stained with osmium tetroxide and flat-embedded in Epon (Fluka). A second vibratome section was also stained with osmium tetroxide and then flat embedded in LR-White-Resin (Hard-Grade Acrylic Resin; London Resin Company). A part of the frontocentral cortex covering all six cortical layers was dissected under microscopic control and pasted on Epon blocks with a drop of Epon. Ultrathin sections were cut at 70 nm. Epon sections were block stained with uranyl acetate and lead citrate, and viewed with a Philips EM400T 120 kV. LR-White sections were immunostained with anti-MAB42 antibodies and visualized with anti-mouse secondary antibodies (Aurion ImmunoGold Reagents & Accessories) labeled with 10 nm nanogold particles. Digital pictures were taken.

Rotarod test. To measure motor coordination, 5- to 7-month-old mice were placed on a horizontal cylinder (Ugo Basile; treadmill for mice Typ 7600) rotating at 13 rounds per minute. The time until the mice fell off the cylinder was measured. Three trials were performed on consecutive days. Trials were terminated after a maximum of 120 s.

Statistical analyses. For statistical analysis, we used Student's *t* tests (two-tailed) or ANOVA followed by Tukey's test for pairwise comparison of all groups as indicated in the figure legends. Rotarod data were

analyzed by Mann–Whitney *U* test followed by Tukey's test; $p < 0.05$ was considered significant for all tests; analyses were done with Systat for Windows 11 (Systat Software) or SPSS 16.0 (SPSS).

Results

Within APP, the N terminus of the Aβ peptide is located in the lumen of the intracellular membrane systems, while its C terminus resides in the center of the transmembrane region (Kang et al., 1987). To insert human $A\beta_{1-40}$ or $A\beta_{1-42}$ in the same membrane orientation during translation at the endoplasmic reticulum, cDNA constructs were made encoding the rat preproenkephalin signal sequence (SPENK) in front of both peptides (Fig. 1*A*). *In vitro* translation of these constructs indicated signal sequence cleavage in the presence of microsomes accompanied by an association of the Aβ peptides with the membrane vesicles (data not shown). Studies with transfected HEK cells had shown approximately equal amounts of $A\beta_{1-40}$ remaining associated with cells and released into the culture medium. In contrast, $A\beta_{1-42}$ largely remained cell associated as also noted by others (Maruyama et al., 1995) (our unpublished data). The murine Thy-1 promoter (Lüthi et al., 1997) was used to drive neuronal expression in brain. For both constructs, the lines with the highest brain Aβ concentration were selected for further studies, APP47 ($A\beta_{1-40}$) and APP48 ($A\beta_{1-42}$).

Aβ expression in APP47 and APP48 mice

The spatial transgene expression pattern in brain was analyzed by *in situ* hybridization (Fig. 1*B*). For both APP47 and APP48 mice, prominent labeling was found in cerebral cortex and hippocampus as expected for the Thy-1 promoter. Other regions including thalamus, cerebellum, and some subcortical nuclei also showed substantial expression. Relative transgene mRNA concentrations in forebrain of young (2-month-old) APP47 and APP48 mice are shown in Figure 1*C*. They were approximately threefold higher for APP47 than for APP48. In double transgenic mice, the expression of both constructs remained unchanged indicating that coexpression did not result in detectable interference of the transgenes.

Young mice were analyzed for Aβ peptides using Western blotting of forebrain homogenates dissolved in SDS-sample buffer (Fig. 2*A*). In contrast to the corresponding mRNA, $A\beta_{1-42}$ reached a considerably higher level than $A\beta_{1-40}$, in agreement with its reduced clearance following brain injection of synthetic peptides (Ji et al., 2001). Quantification of the Aβ peptides after formic acid extraction indicated a ~10-fold higher steady-state concentration of $A\beta_{42}$ than $A\beta_{40}$ (Fig. 2*B*). Interestingly, in APP47 × APP48 mice, $A\beta_{42}$ was reduced by ~75% compared with single transgenic mice, while $A\beta_{40}$ was elevated ~2.5-fold. The absolute concentrations of both peptides were very similar, suggestive of an interaction.

The identity of the Aβ peptides in APP47 and APP48 mice was confirmed by MALDI-TOF analysis following immunoprecipitation of SDS-dissolved forebrain extracts (Fig. 2*C*). The molecular weights determined for the Aβ peaks in both transgenic lines were in agreement with the full-length $A\beta_{1-40}$ and $A\beta_{1-42}$ peptides, respectively. These data demonstrate the proper cleavage of the signal sequence. No other Aβ peptides were detectable. SDS gels in addition showed one or two faster migrating bands, most notably in APP47 × APP48 mice, which varied in amount but always remained minor forms (Fig. 2*D*). The upper band comigrated with $A\beta_{2-42}$ and the lower one with $A\beta_{4-40/42}$ and pyroglutamate Aβ ($N3pEA\beta_{3-40/42}$). To further characterize the lower band, Aβ was immunoprecipitated from forebrain homogenates followed by Western blotting with an N3pEAβ antibody. Only

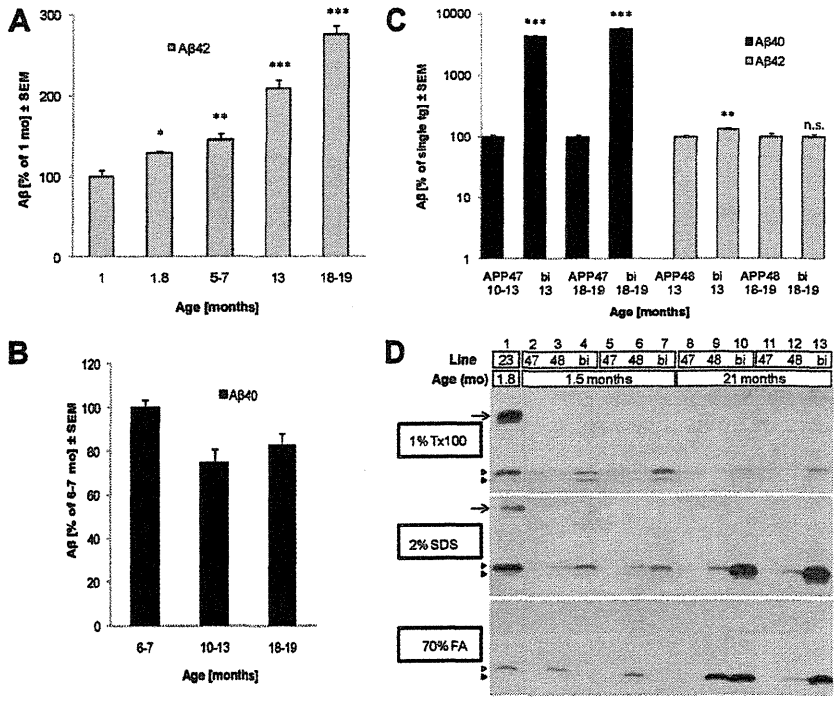

Figure 3. Age-dependent changes and solubility characteristics of brain Aβ in APP47 and APP48 mice. Formic acid-extracted total $A\beta_{40}$ and $A\beta_{42}$ in cerebral cortex was analyzed at the indicated ages using electrochemoluminescence assays. ***A***, The $A\beta_{42}$ concentration in APP48 brain significantly increased with age (Student's *t* test vs 1 month, two-tailed) as indicated by asterisks: $*p < 0.05$, $**p < 0.01$, $***p < 0.001$. Linear regression analysis (regression ANOVA $F_{(1,32)} = 317.7, p < 0.001$) indicated age as a strong and linear determinant of $A\beta_{42}$. ***B***, The $A\beta_{40}$ concentration in APP47 mouse brain remained unchanged ($p > 0.05$, Student's *t* test, two-tailed, and linear regression). ***C***, Compared with APP47, $A\beta_{40}$ was considerably elevated in aged APP47 × APP48 mice, whereas $A\beta_{42}$ was not consistently different from APP48 (Student's *t* test vs single-transgenic mice, two-tailed). Error bars indicate SEM. ***D***, Forebrain homogenates of 1.5- and 21-month-old APP47, APP48, and APP47 × APP48 (bi) mice were sequentially extracted with 1% Triton X-100, 2% SDS, and 70% formic acid. Extracts were immunoprecipitated with antibody 4G8 and analyzed by Western blotting with antibody 6E10, both directed against Aβ. A gel without urea was used, which does not separate $A\beta_{1-40}$ and $A\beta_{1-42}$. The faster migrating band corresponds to the truncated Aβ isoforms separated on SDS/urea gels (see above). This band is primarily found in the Triton and SDS extracts from young mice. An extract from a young APP transgenic mouse (APP23) is shown for comparison.

Table 1. Average forebrain weight of APP47, APP48, and double-transgenic mice at 2 and 21 months of age

Age group	Wild type	APP47	APP48	APP47 × APP48
2 months				
Forebrain weight (mg)[a]	164 ± 10	165 ± 9	152 ± 10	152 ± 7
p (vs wild type)*		NS	0.006	0.002
21 months				
Forebrain weight (mg)[a]	161 ± 10	154 ± 9	132 ± 8	131 ± 10
p (vs wild type)*		NS	<0.0001	<0.0001

[a]Shown are mean ± SD.

*Student's *t* test, two-tailed. NS, Nonsignificant.

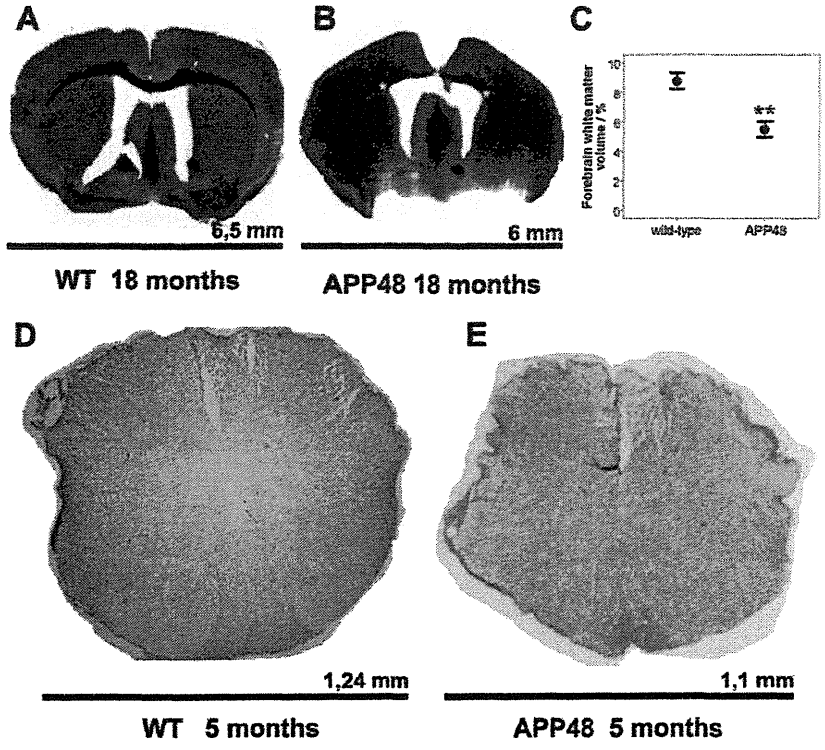

Figure 4. Macroscopic analysis of brains from APP48 mice. The forebrain of APP48 (*B*) mice was ~10% smaller than that of wild-type mice (*A*) as measured by the bi-hemispheric diameter, which is indicated as black bar below the brain section. The relative forebrain white matter volume was decreased in APP48 mice as seen morphologically in the central white matter and the corpus callosum (*B*, stars) and as documented by quantitative assessment (Student's *t* test, two-tailed, $^{**}p < 0.01$; *C*). *D*, *E*, The spinal cord was also ~10% smaller in APP48 mice (*E*) than in wild-type mice (*D*). However, morphological changes and especially white matter loss did not become obvious.

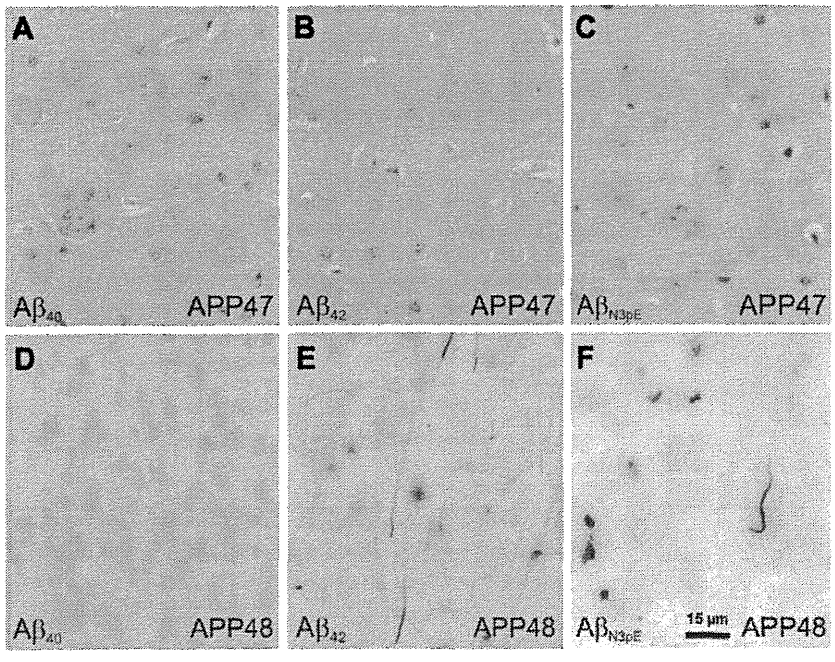

Figure 5. N3pEAβ staining in APP47 and APP48 mice. Neocortical sections from 18-month-old APP47 (*A–C*) and APP48 (*D*, *E*) mice were immunostained with antibodies specific for $A\beta_{40}$ (*A*, *D*), $A\beta_{42}$ (*B*, *E*), or N3pEAβ (*C*, *F*). As expected, APP47 brains were stained with $A\beta_{40}$ but not $A\beta_{42}$ antibodies, whereas APP48 reacted with $A\beta_{42}$ but not $A\beta_{40}$ antibodies. Pyroglutamate was found in neuropil Aβ grains and few dendritic Aβ treads but not in somatic Aβ granules of APP48 but not in APP47 mice. Scale bar, 15 μm.

after prolonged exposure was a band detectable in 21-month-old APP47 × APP48 mouse brains but not young double transgenic or the single-transgenic brains. In contrast, Aβ antibody 6E10 recognized the lower band to almost the same extent in young and old animals. Sequential immunoprecipitation with the N3pE followed by the 6E10 Aβ antibodies confirmed that only a minor Aβ fraction in this band contained pyroglutamate (data not shown). The main portion of the lowest band most likely corresponded to $A\beta_{4-40/42}$ in agreement with the lack of detection by antibody β1 against the $A\beta_{3-6}$ epitope (data not shown).

Age-related increase of insoluble $A\beta_{42}$ but not $A\beta_{40}$

To estimate the overall changes with age, total $A\beta_{42}$ in APP48 mice was analyzed after formic acid extraction of the cerebral cortex. An approximately threefold increase was found between 1 and 19 months of age (Fig. 3*A*). By contrast, $A\beta_{40}$ in APP47 mice remained at a similar level during aging (Fig. 3*B*). In aged double-transgenic APP47 × APP48 mice, $A\beta_{40}$ increased considerably compared with APP47 alone, while $A\beta_{42}$ reached the same level as found in APP48 (Fig. 3*C*).

These results and the discrepancy between mRNA and protein steady-state levels of $A\beta_{40}$ and $A\beta_{42}$ prompted us to analyze their solubility. Whereas Triton X-100 extraction almost completely solubilized $A\beta_{40}$ from APP47 brains, $A\beta_{42}$ in APP48 brain remained largely in the insoluble pellet after Triton X-100 and SDS extraction (data not shown). For more systematic analysis, forebrains from young and aged animals (1.5 and 21 months of age) were sequentially extracted with Triton X-100, SDS, and formic acid and analyzed by Western blotting (Fig. 3*D*). Regardless of the age, the initial Triton X-100 treatment completely extracted $A\beta_{40}$ from APP47 brain. In contrast, Triton X-100 hardly dissolved any $A\beta_{42}$ either from young or aged APP48 brains. $A\beta_{42}$ mostly distributed between the SDS and formic acid extracts. This is consistent with the very low level of $A\beta_{42}$ secretion from cells transfected with the same construct. Young APP47 × APP48 mice showed increased Aβ about equally distributed between the Triton X-100- and SDS-soluble fractions. Aβ in the SDS-insoluble material was hardly detectable. It increased considerably in this and the SDS fraction at old age, while the Triton X-100-soluble Aβ remained constant or decreased slightly. The complete extraction of the Aβ peptides in every step required large buffer

volumes and 2% SDS/sonication in the second step. Smaller extraction volumes or less harsh SDS treatment reduced the Aβ peptides in the corresponding fractions with a concomitant increase in the following extracts (data not shown). Independent of the extraction conditions, these data demonstrate an age-related increase of insoluble $A\beta_{42}$. Such an increase did not occur with $A\beta_{40}$ alone but was detectable in the presence of $A\beta_{42}$ (Fig. 3*D*). Aβ from a young APP23 transgenic mouse (APP with Swedish mutation) analyzed in parallel distributed between all fractions.

Distinct neuropathology after intracellular $A\beta_{42}$ expression

The forebrain weights of the different mouse lines were compared at 2 and 21 months of age. No significant difference from wild-type mice was found for APP47. However, APP48 mice showed a reduction in forebrain weight at 2 months, which became more pronounced with age. The same reduction was observed for double-transgenic mice of the corresponding age groups (Table 1). Further investigation of APP48 mice showed a reduced bihemispheric diameter in forebrain compared with wild-type animals (Fig. 4*A*,*B*). Quantitative analysis demonstrated a ~37% reduction in white matter volume (Fig. 4*C*). A slightly reduced overall size (~10%) was observed for the spinal cord (Fig. 4*D*,*E*) without other obvious changes.

Analyses of APP47 brains by Aβ immunohistochemistry demonstrated weak staining of $A\beta_{40}$ granules in the soma of neurons (Fig. 5*A–C*). N3pEAβ (pyroglutamate-Aβ) was not detected. Amyloid plaques or other signs of histopathology were not found even at the oldest age analyzed (24 months).

Immunohistochemistry did not detect amyloid plaques in APP48 mice even at the age of 24 months. Instead, three types of lesions were stained with different Aβ antibodies (MBC42, 4G8, NT11, AβN1D): (1) dendrites filled with Aβ-positive material of thread-like appearance (dendritic Aβ threads), (2) dot-like granules in the soma of nerve cells (somatic Aβ granules), and (3) grain-like structures in the neuropil (Aβ grains) (Figs. 5*E*, 6*A–G*). The three types of Aβ lesions were found throughout the entire gray matter of the CNS. Their distribution varied among different CNS regions with the most severe pathology in neocortical and allocortical areas (Table 2). Aβ threads were less frequently found in the brainstem and cerebellum and were not seen in the spinal cord, whereas Aβ granules were found in all these regions (Fig. 6*I*,*J*). Staining with an N3pEAβ antibody visualized Aβ grains, few dendritic Aβ threads, but no somatic Aβ granules (Fig. 5*E*,*F*). Aβ-positive lesions in APP48 mice were not stained with an $A\beta_{40}$ antibody (Fig. 5*D*).

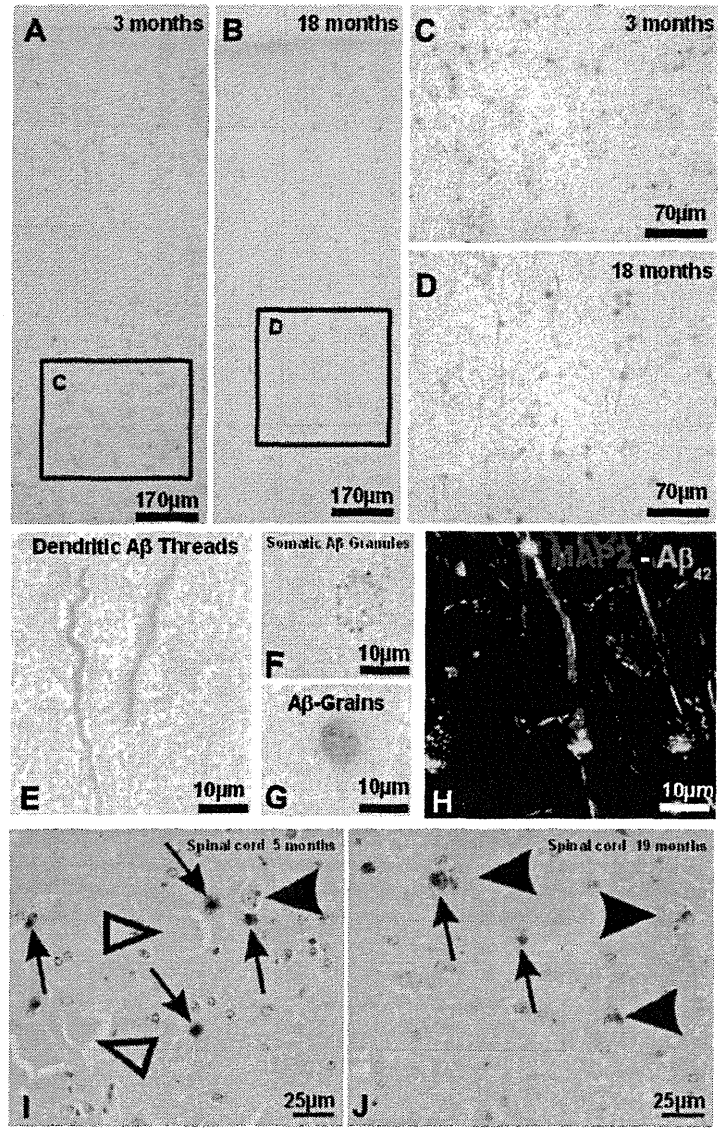

Figure 6. Aβ lesions in APP48 mice. ***A***, ***B***, In the neocortex, Aβ changes were mainly located in layers II, III, V, and VI in 3- as well as in 18-month-old animals. No amyloid plaques were visible. ***C***, At 3 months of age, Aβ antibodies predominantly stained grain-like structures, whereas thread-like material and somatic granules were less frequently found. ***D***, In 18-month-old APP48 mice, thread-like lesions predominated, while grains and granules became less abundant (see Fig. 8 for quantification). ***E–G***, Higher magnification of the three major Aβ accumulations in APP48 mice: dendritic Aβ threads (***E***) representing dendrites filled with Aβ; somatic Aβ granules (***F***), which are dot-like Aβ-positive structures within the perikaryon of neurons. They were distributed in the cell soma; Aβ grains (***G***) representing extraneuronal accumulations of Aβ. ***H***, Double-label immunofluorescence for Aβ and MAP2 confirmed the dendritic localization of the Aβ threads. These three Aβ lesions are found throughout the gray matter of the CNS, although Aβ threads were missing in the spinal cord (***I***, ***J***). ***I***, At 5 months of age, Aβ grains were predominant (arrows). Only few interneurons with somatic granules were observed (black arrowhead). Motor neurons were free of Aβ (open arrowheads). ***J***, At 19 months of age, somatic granules were also seen in motor neurons (arrowheads) and Aβ grains were less abundant (arrows).

Double-label immunohistochemistry corroborated the presence of Aβ in MAP2-positive dendrites of APP48 mice (Fig. 6*H*). Campbell–Switzer silver staining indicated a fibrillar structure of dendritic Aβ with the pattern of threads (Fig. 7*A*). Ultrastructurally, the dendritic Aβ-positive material showed a fibril-like appearance (Fig. 7*B*,*C*). Axonal Aβ was not observed. The intracellular location of somatic Aβ granules was further analyzed by immuno-electron microscopy, which detected Aβ-positive material in lysosomes of neurons (Fig. 7*D*,*E*). Neuropil grains were associated with CD45-positive microglial cells (Fig.

Table 2. Distribution of morphological changes in APP48 mice

Brain regions	Conventional histology	$A\beta_{42}$ staining
Neocortex	—	Aβ grains, Aβ granules, Aβ threads
Allocortex (including hippocampus)	Reduction of neurons in CA1	Few Aβ grains, Aβ granules, Aβ threads
Basal ganglia	—	Aβ grains, Aβ threads
Thalamus	—	Aβ grains, Aβ granules, and few Aβ threads
Basal forebrain nuclei	—	Aβ granules, single Aβ threads, and Aβ grains in aged animals
Midbrain	—	Aβ granules, single Aβ threads, and Aβ grains in aged animals
Brainstem	—	Aβ granules, single Aβ threads, and Aβ grains in aged animals
Cerebellum: dentate nucleus	—	Aβ granules, single Aβ threads, and Aβ grains in aged animals
Cerebellum: granule cell layer	—	Aβ grains
Cerebellum: Purkinje cells	—	—
Spinal cord	Reduction of spinal cord diameter	Aβ grains, Aβ granules
Cerebral, cerebellar, and spinal white matter	Reduction of cerebral white matter in aged animals	—

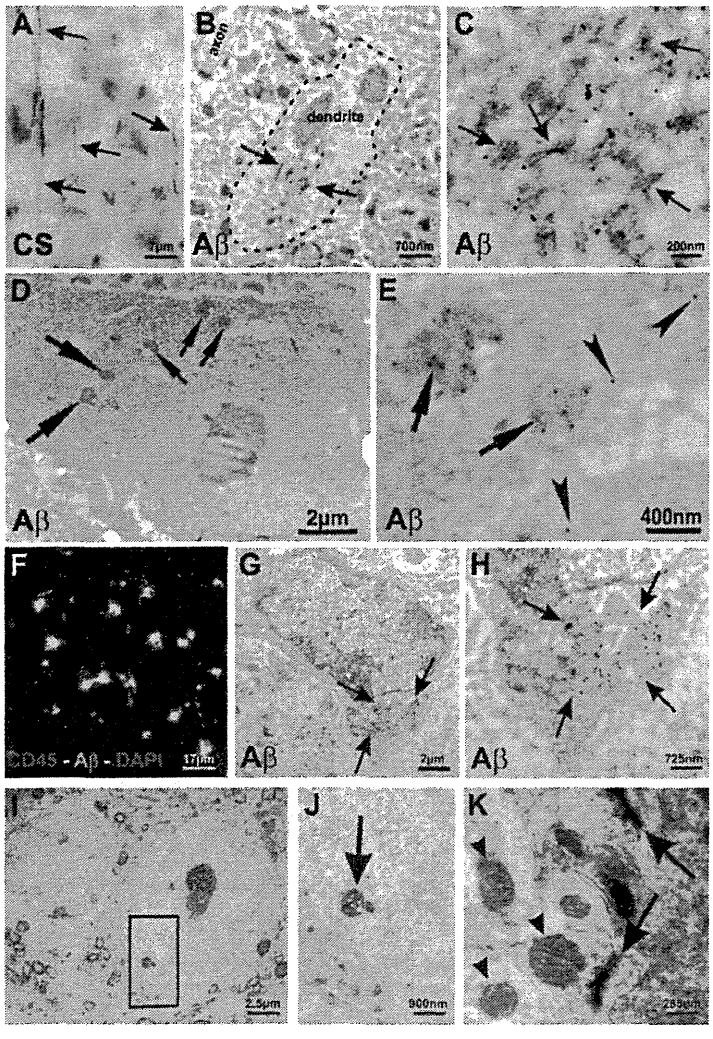

Figure 7. Immuno-electron-microscopic localization of Aβ lesions and ultrastructural analyzes. ***A***, Campbell–Switzer silver staining of dendritic Aβ threads indicated the fibrillar nature of the aggregates (arrows). ***B***, At the immuno-electron-microscopic level, a distinct number of dendrites (example marked by the dashed line) in the neuropil of the frontocentral neocortex contained Aβ-positive material (arrows). Note that the axon did not contain Aβ. ***C***, At higher magnification, the Aβ-positive dendritic material exhibited a fibrillar structure (arrows) consistent with the SDS resistance of an $A\beta_{1-42}$ subpopulation. ***D***, Immuno-electron microscopy showed a neuron with somatic Aβ granules. ***E***, Higher magnification (area of the top two arrows in ***D***) detected Aβ within lysosomes (arrows) and more rarely in the endoplasmic reticulum (arrowheads). ***F***, Double-label immunofluorescence indicated that Aβ grains (labeled in green) were associated with CD45-positive microglial cells. ***G***, Using immuno-electron microscopy, microglial cells were found, which exhibited lysosomal $A\beta_{42}$-reactive material. ***H***, Higher magnification of the lysosomal region outlined by arrows. ***I–K***, Epon-embedded tissue exhibited a better structural resolution than the immuno-electron material. ***I***, Neurons did not show obvious alterations of their subcellular organization. ***J***, No specific changes were found in lysosomes (arrow) at higher magnification (***I***, frame). ***K***, Dendrites and synapses appeared normal. Mitochondria (arrowheads) within the dendrites and axons showed no obvious changes (arrows indicate dendritic threads).

7*F*). Immuno-electron microscopy confirmed the microglial Aβ inclusions and indicated a lysosomal association (Fig. 7*G*,*H*). We did not observe Aβ in multivesicular bodies of APP48 mice but found minor staining in the endoplasmic reticulum (Fig. 7*E*, arrowheads).

Double-labeling immunofluorescence showed colocalization of neuronal Aβ granules and microglial Aβ grains with BIP and LAMP-1 in agreement with a late endosomal/lysosomal localization of both structures (Fig. 8*A–I*). Dendritic Aβ threads did not colocalize with BIP and LAMP-1, further indicating that these aggregates are different from Aβ granules and grains (Fig. 8*J–L*). No colocalization was found with markers for early endosomes (EEA1) and stress granules [TIA/TIAR(D-9)] (data not shown).

Structural analysis in Epon-embedded sections by electron microscopy revealed few lysosomal, lipofuscin-like aggregates in the soma of neurons (Fig. 7*I*,*J*). Further structural changes, especially in dendrites, were neither detected at the ultrastructural (Fig. 7*K*) nor at the light-microscopic level. Immunohistochemisty did not show alterations of the dendritic tree or of axons in neurofilament-stained sections of 3- and 18-month-old APP48 mice when comparing with age-matched wild-type animals. Dystrophic neurites were not observed in the APP staining. The cortical distribution of synaptophysin-positive material did not differ between APP48 and wild-type mice. Abnormally phosphorylated tau and pTDP-43 were not found in the brains of APP48 mice. There were no obvious differences in the distribution pattern of GFAP-positive astrocytes and RCA-positive microglial cells between wild-type and APP48 mice. APP47 × APP48 mice showed qualitatively similar alterations as APP48.

Quantification of the three Aβ lesions in the frontocentral cortex of APP48 mice (Fig. 9*A–C*) revealed an approximately

threefold increase in the number of dendritic Aβ threads between 3 and 18 month of age. In contrast, an age-dependent ~45–48% decrease of Aβ granules and grains was found. The frontocentral neocortex did not show alterations in neuron number compared with wild-type mice (Fig. 9*D*). However, we found considerable neuron loss in the hippocampus at 3 and 18 months of age (Fig. 9*E*).

Motor deficit in APP48 mice

Compared with wild-type animals the APP47 genotype had no significant effect on body weight, while it was reduced in APP48 at 12 to 15 months (Table 3). Inspection over time showed no difference from wild type at 1 month but a body weight reduction from 2 months onward. An intermediate weight was found for double-transgenic APP47 × APP48 mice. APP48 but not APP47 mice presented with minor motor anomalies at ~6 months, which increased with age, and occasionally paralysis developed above 18 months of age. No increase in spontaneous mortality was apparent in these mouse lines.

To evaluate the apparent motor deficit quantitatively, 5- to 7-month-old APP48 were analyzed in the Rotarod test compared with littermate controls (Fig. 10). During three consecutive trials done, APP48 mice fell off the rod much more quickly than the controls. These data indicate a considerable impairment in motor coordination in aged APP48 mice.

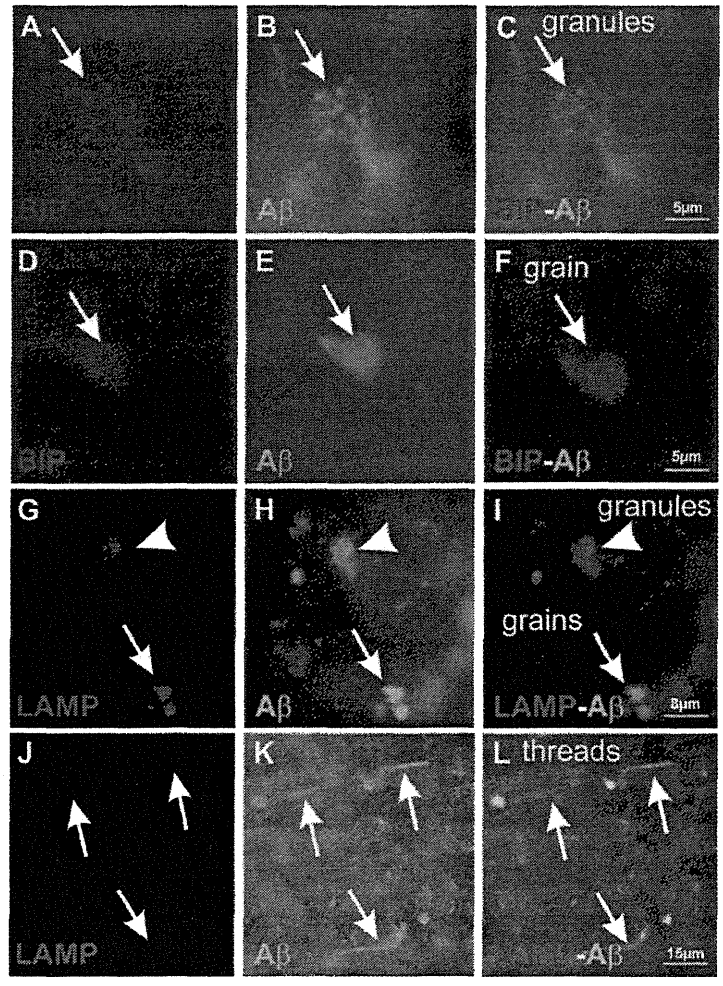

Figure 8. Localization of Aβ lesions at intracellular membrane compartments by double immunolabeling. Double-label immunohistochemistry for BIP (***A***, ***D***), a marker of post-endoplasmatic reticulum compartments, and Aβ (***B***, ***E***) showed colocalization of BIP and Aβ (***C***, ***F***) in Aβ granules (***A–C***, arrow) and microglial Aβ grains (***D–F***, arrow). The lysosomal marker LAMP-1 (***G***) demonstrated a similar colocalization (***I***) with Aβ (***H***) in granules (arrowhead) and grains (arrow) as BIP, indicating their lysosomal location. Aβ labeling (***K***) of dendritic threads (***J–L***, arrows) did not colocalize (***L***) with the lysosomal marker LAMP-1 (***J***), further distinguishing Aβ threads from Aβ granules and grains.

Discussion

In the present study, we describe transgenic mouse lines expressing $A\beta_{1-40}$ (APP47) and $A\beta_{1-42}$ (APP48) in neurons. The expression constructs encode a signal sequence to insert both Aβ peptides into the endoplasmic reticulum presumably with a similar orientation as after cleavage from APP. In contrast to regular cleavage of Aβ from APP, which largely occurs in endosomes and is followed by rapid secretion (Selkoe et al., 1996), the Aβ peptides are synthesized in the endoplasmic reticulum. Cell culture studies have shown substantial amounts of intracellular Aβ and comparably little secretion in particular of $A\beta_{1-42}$ (Maruyama et al., 1995) (our unpublished data).

Brains from young APP48 mice contained considerably more Aβ than the corresponding APP47 brains, while the inverse was true on the mRNA level. Different translational efficacies of these very similar constructs appear unlikely. Moreover, the mRNA levels remained unchanged in APP47 × APP48 mice relative to the parent lines, whereas the amount of both Aβ isoforms was considerably altered. This argues in favor of a differential post-translational regulation of the Aβ isoforms. A higher clearance of $A\beta_{1-40}$ has been observed after brain injection (Ji et al., 2001), and this more soluble peptide may also undergo faster intracellular degradation. Accordingly, $A\beta_{1-40}$ in APP47 mice remained at a similar level during aging, whereas $A\beta_{1-42}$ showed a moderate elevation in APP48 mice.

$A\beta_{1-42}$ seems able to stabilize $A\beta_{1-40}$ albeit at the expense of its own stability. In young APP47 × APP48 mice, $A\beta_{1-42}$ was decreased and more soluble while $A\beta_{1-40}$ was increased compared with the parent lines. The relative ratio of both peptides may strongly influence their stability as indicated by a recent *in vitro* study (Kuperstein et al., 2010). During aging of APP47 × APP48 mice, $A\beta_{1-42}$ increased moderately just compensating the decrease at young age compared with the single-transgenic mice (APP48). For $A\beta_{1-40}$, a very large increase was found in double- compared with single-transgenic mice (APP47). Consistent with an intracellular interaction of both Aβ peptides, no such effect on the steady-state levels was observed when both peptides were fused to the C terminus of the BRI protein and rapidly secreted after cleavage (Kim et al., 2007). However, intracellular Aβ cannot be completely excluded in these mice as its analysis has not been a topic of the study. Nonetheless, secreted $A\beta_{1-40}$ inhibited amyloid deposition in APP transgenic mice, which indicates an extracellular interaction affecting overall solubility of the Aβ peptides.

Among the lines, APP48 mice develop the more advanced pathology and show three types of Aβ lesions. Neurons contain

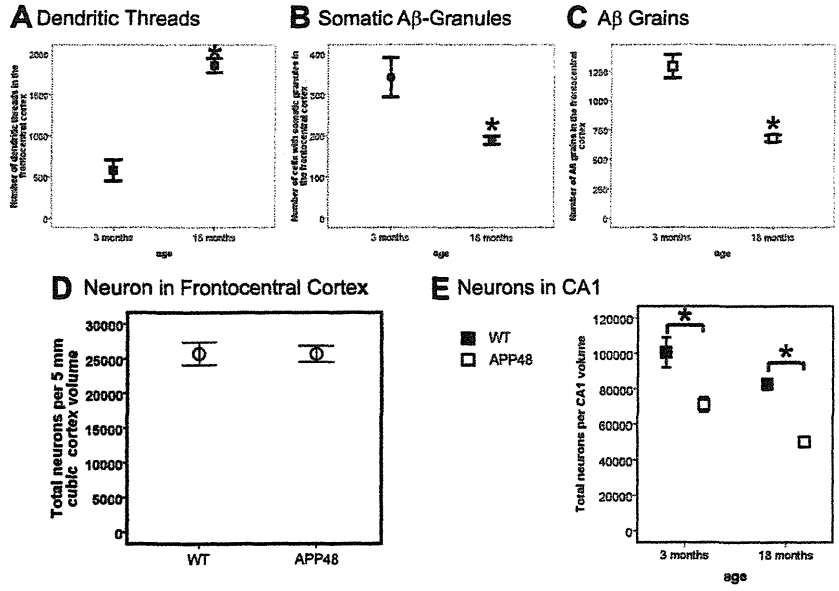

Figure 9. Quantification of Aβ lesions and neuron numbers in APP48 mice. Dendritic Aβ threads (***A***), somatic Aβ granules (***B***), and microglia Aβ grains (***C***) were quantified in the frontocentral neocortex of 3- and 18-month-old APP48 mice. This analysis revealed an increase in the number of dendritic Aβ threads with age but a decrease of somatic Aβ granules and microglial Aβ grains. Stereology was used to quantify neurons in the frontal cortex (***D***) of 18-month-old APP48 mice compared with wild-type littermate controls, which did not show a difference ($p = 0.613$). The total number of neurons was reduced in hippocampus (***E***) at both 3 and 18 months of age. Significant differences are indicated (Student's *t* test, two-tailed, $*p < 0.05$).

Table 3. Average body weight of APP47, APP48, and double-transgenic mice at 12–15 months of age

Gender	Body weight	Wild type	APP47	APP48	APP47 × APP48
Females	Body weight (g)[a]	39 ± 5	38 ± 5	23 ± 3	30 ± 5
	p (vs wild type)*		NS	<0.0001	<0.0001
Males	Body weight (g)[a]	45 ± 10	41 ± 6	30 ± 4	36 ± 5
	p (vs wild type)*		NS	<0.0001	<0.005

[a]Shown are mean ± SD.

*Student's *t* test, two-tailed. NS, Nonsignificant.

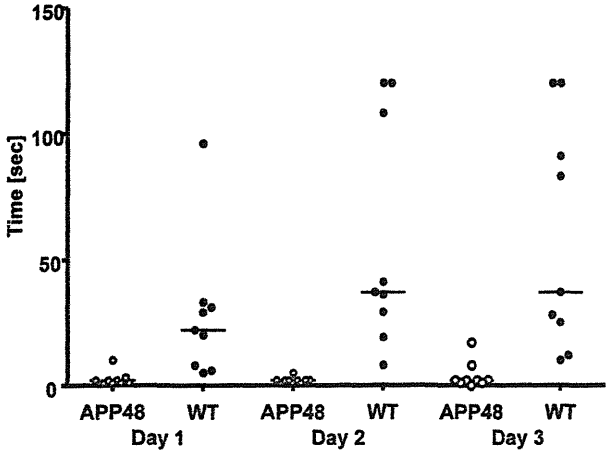

Figure 10. Motor impairment of APP48 mice. APP48 mice (open circles) and littermate controls (closed circles) at the age of 5–7 months were evaluated in the Rotarod test on 3 consecutive days. The time on the rod is shown for each individual animal, and the median is indicated. In all three tests, APP48 mice stayed significantly less long on the rod than the controls (Mann–Whitney *U* test; trial 1, $p < 0.001$; trial 2, $p < 0.0003$; trial 3, $p < 0.0007$).

Aβ threads in dendrites and somatic Aβ granules in lysosomes. Additionally, Aβ grains are present in lysosomes of microglia cells. Dendritic Aβ threads appear fibrillar at the electron-microscopic level and can be silver stained. They accumulate with age possibly because their fibrillar structure prevents efficient degradation. In contrast, $A\beta_{1-42}$ found as granules in neuronal lysosomes neither appears fibrillar nor shows other evidence of accumulation, suggesting that it may be degraded. With progressing dendritic Aβ aggregation, an increased number of assembly sites becomes available. These changes may lead to a shift of Aβ toward dendritic threads and a reduced lysosomal transport resulting in the observed decrease of Aβ granules with age. The detection of Aβ in dendrites and lysosomes demonstrates that the peptide is transported within the neuron from the site of synthesis at the endoplasmic reticulum to other locations. The small Aβ signal in the endoplasmic reticulum observed at the electron-microscopic level is in agreement with the synthesis of Aβ at this location. We did not detect Aβ in multivesicular bodies as described for APP transgenic mice and AD brain (Takahashi et al., 2002). APP47 mice only show somatic Aβ granules consistent with a more rapid and complete degradation of $A\beta_{1-40}$.

In APP48 brain, Aβ is also found in microglial lysosomes even though the Thy-1 cassette drives expression in neurons (Calhoun et al., 1999). It may derive from Aβ secretion known to occur to a certain extent in cell culture. Alternatively, microglial Aβ may originate from degenerated neurons or neuronal processes, but the lack of PAS-positive lysosomal/lipofuscin-like material and the absence of phagosomes at the electron-microscopic level argue against strong phagocytosis. Interestingly, the very small amount of pyroglutamate Aβ is mainly associated with microglial but not neuronal lysosomes, indicating that pyroglutamate-Aβ (N3pEAβ) formation is largely avoided when Aβ is directly targeted for degradation. In agreement with a slow conversion of $A\beta_{1-42}$ to pyroglutamate Aβ, this isoform was also detected in dendritic threads.

Intracellular Aβ in APP47 and APP48 mice does not lead to amyloid plaque formation, although the total brain Aβ concentrations are comparable with preplaque APP transgenic mice, which form plaques during aging (Abramowski et al., 2008). Intracellular membrane expression and aggregation of Aβ as in APP48 is apparently not sufficient for plaque formation. This does not exclude that plaque development requires Aβ generation and aggregation in a specific intracellular location, which is reached by APP or its C-terminal fragments but not by Aβ as it lacks the trafficking signals. However, intraneuronal Aβ accumulation in the absence of extracellular amyloid plaques has also been observed in transgenic mice expressing APP with the AD-linked E693Δ mutation (Tomiyama et al., 2010). In contrast, amyloid plaque formation has been observed in $A\beta_{1-42}$ transgenic mice using the BRI protein as vehicle to secrete the Aβ peptides (McGowan et al., 2005). Together, the studies favor the notion that amyloid plaques are formed after secretion of Aβ. Single diffuse plaques have also been observed in $A\beta_{3-42}$ trans-

genic mice, which produce considerable N3pEAβ (Wirths et al., 2009). The strong tendency of N3pEAβ to aggregate (Schlenzig et al., 2009) in combination with a low level of secretion may be sufficient for plaque formation.

We did not observe further structural changes associated with dendritic Aβ threads and lysosomal granules or grains. It is possible that dendritic threads or potential related soluble Aβ aggregates impair neuronal function in the absence of further structural changes. The pathological significance of increased lysosomal Aβ in granules and grains is less clear, and their reduction during aging argues against a role in degeneration or functional impairment. APP48 mice show a dramatically reduced neuron number in hippocampus, but no such change was detectable in frontal cortex. A similar discrepancy has been found in APP23 mice (Calhoun et al., 1998) and may be related to the higher vulnerability of hippocampal neurons. Additionally, APP48 mice loose brain weight, apparently due to a severe white matter reduction. These findings suggest a loss of myelinated axons in the absence of extensive pathology as observed in AD and other neurodegenerative diseases (Ihara et al., 2010). The white matter atrophy may be mainly explained by the severe hippocampal neuron loss. These neurons project to other cortical areas constituting a significant number of axons in the white matter. No obvious loss of neurons involved in motor function and coordination was found, which would explain the motor deficits observed in APP48. However, degeneration of axons from such neurons or their functional impairment appears possible in view of the fibrillar Aβ thread pathology in neurons relevant for motor function and coordination (motor cortex, basal ganglia, and cerebellar dentate nucleus). A primary alteration of spinal motor neurons seems less likely because skeletal muscles did not exhibit the pattern of spinal muscular atrophy.

Hippocampal neuron loss is already present at 3 months of age and does not progress much further. It appears that most of the detectable toxicity of intracellular Aβ occurs shortly after postnatal onset of strong Thy-1 promoter expression. Compared with APP transgenic mice, APP48 develop an overlapping but distinct pathology. None of these models including BRI-Aβ mice (McGowan et al., 2005) develops most of the non-Aβ pathology typical of AD. In all systems including AD brain, Aβ aggregates do not show strong acute toxicity but may lead to a slow deregulation of neuronal networks (Palop and Mucke, 2010). The APP48 animal model described here indicates that $A\beta_{1-42}$ generated at the luminal membrane side can form intracellular Aβ aggregates and induce some neurodegeneration, most notably in hippocampus, white matter atrophy, and motor deficits.

References

Abramowski D, Wiederhold KH, Furrer U, Jaton AL, Neuenschwander A, Runser MJ, Danner S, Reichwald J, Ammaturo D, Staab D, Stoeckli M, Rueeger H, Neumann U, Staufenbiel M (2008) Dynamics of A beta turnover and deposition in different beta-amyloid precursor protein transgenic mouse models following gamma-secretase inhibition. J Pharmacol Exp Ther 327:411–424.

Braak H (1974) On the structure of the human archicortex. I. The cornu ammonis. A Golgi and pigmentarchitectonic study. Cell Tissue Res 152:349–383.

Braak H, Braak E (1991) Demonstration of amyloid deposits and neurofibrillary changes in whole brain sections. Brain Pathol 1:213–216.

Calhoun ME, Wiederhold KH, Abramowski D, Phinney AL, Probst A, Sturchler-Pierrat C, Staufenbiel M, Sommer B, Jucker M (1998) Neuron loss in APP transgenic mice. Nature 395:755–756.

Calhoun ME, Burgermeister P, Phinney AL, Stalder M, Tolnay M, Wiederhold KH, Abramowski D, Sturchler-Pierrat C, Sommer B, Staufenbiel M, Jucker M (1999) Neuronal overexpression of mutant amyloid precursor protein results in prominent deposition of cerebrovascular amyloid. Proc Natl Acad Sci U S A 96:14088–14093.

Capetillo-Zarate E, Staufenbiel M, Abramowski D, Haass C, Escher A, Stadelmann C, Yamaguchi H, Wiestler OD, Thal DR (2006) Selective vulnerability of different types of commissural neurons for amyloid β-protein-induced neurodegeneration in APP23 mice correlates with dendritic tree morphology. Brain 129:2992–3005.

Citron M (2010) Alzheimer's disease: strategies for disease modification. Nat Rev Drug Discov 9:387–398.

Gouras GK, Tampellini D, Takahashi RH, Capetillo-Zarate E (2010) Intraneuronal beta-amyloid accumulation and synapse pathology in Alzheimer's disease. Acta Neuropathol 119:523–541.

Hsu SM, Raine L, Fanger H (1981) Use of avidin-biotin-peroxidase complex (ABC) in immunoperoxidase techniques: a comparison between ABC and unlabeled antibody (PAP) procedures. J Histochem Cytochem 29:577–580.

Ihara M, Polvikoski TM, Hall R, Slade JY, Perry RH, Oakley AE, Englund E, O'Brien JT, Ince PG, Kalaria RN (2010) Quantification of myelin loss in frontal lobe white matter in vascular dementia, Alzheimer's disease, and dementia with Lewy bodies. Acta Neuropathol 119:579–589.

Jack CR Jr, Knopman DS, Jagust WJ, Shaw LM, Aisen PS, Weiner MW, Petersen RC, Trojanowski JQ (2010) Hypothetical model of dynamic biomarkers of the Alzheimer's pathological cascade. Lancet Neurol 9:119–128.

Ji Y, Permanne B, Sigurdsson EM, Holtzman DM, Wisniewski T (2001) Amyloid beta40/42 clearance across the blood-brain barrier following intra-ventricular injections in wild-type, apoE knock-out and human apoE3 or E4 expressing transgenic mice. J Alzheimers Dis 3:23–30.

Kang J, Lemaire HG, Unterbeck A, Salbaum JM, Masters CL, Grzeschik KH, Multhaup G, Beyreuther K, Müller-Hill B (1987) The precursor of Alzheimer's disease amyloid A4 protein resembles a cell-surface receptor. Nature 325:733–736.

Kim J, Onstead L, Randle S, Price R, Smithson L, Zwizinski C, Dickson DW, Golde T, McGowan E (2007) Aβ40 inhibits amyloid deposition *in vivo*. J Neurosci 27:627–633.

Klafki HW, Wiltfang J, Staufenbiel M (1996) Electrophoretic separation of betaA4 peptides (1–40) and (1–42). Anal Biochem 237:24–29.

Kuperstein I, Broersen K, Benilova I, Rozenski J, Jonckheere W, Debulpaep M, Vandersteen A, Segers-Nolten I, Van Der Werf K, Subramaniam V, Braeken D, Callewaert G, Bartic C, D'Hooge R, Martins IC, Rousseau F, Schymkowitz J, De Strooper B (2010) Neurotoxicity of Alzheimer's disease Abeta peptides is induced by small changes in the Abeta42 to Abeta40 ratio. EMBO J 29:3408–3420.

Lüthi A, Van der Putten H, Botteri FM, Mansuy IM, Meins M, Frey U, Sansig G, Portet C, Schmutz M, Schröder M, Nitsch C, Laurent JP, Monard D (1997) Endogenous serine protease inhibitor modulates epileptic activity and hippocampal long-term potentiation. J Neurosci 17:4688–4699.

Maruyama K, Tagawa K, Kawamura Y, Asada H, Ishiura S, Obata K (1995) Secretion of Alzheimer beta/A4 protein (1–40) and intracellular retention of beta/A4 protein (1–42) in transfected COS cells. Biochem Biophys Res Commun 207:971–977.

McGowan E, Pickford F, Kim J, Onstead L, Eriksen J, Yu C, Skipper L, Murphy MP, Beard J, Das P, Jansen K, Delucia M, Lin WL, Dolios G, Wang R, Eckman CB, Dickson DW, Hutton M, Hardy J, Golde T (2005) Abeta42 is essential for parenchymal and vascular amyloid deposition in mice. Neuron 47:191–199.

Nimmrich V, Ebert U (2009) Is Alzheimer's disease a result of presynaptic failure? Synaptic dysfunctions induced by oligomeric beta-amyloid. Rev Neurosci 20:1–12.

Palop JJ, Mucke L (2010) Amyloid-beta-induced neuronal dysfunction in Alzheimer's disease: from synapses toward neural networks. Nat Neurosci 13:812–818.

Reichwald J, Danner S, Wiederhold KH, Staufenbiel M (2009) Expression of complement system components during aging and amyloid deposition in APP transgenic mice. J Neuroinflammation 6:35.

Saido TC, Iwatsubo T, Mann DM, Shimada H, Ihara Y, Kawashima S (1995) Dominant and differential deposition of distinct beta-amyloid peptide species, A beta N3(pE), in senile plaques. Neuron 14:457–466.

Schlenzig D, Manhart S, Cinar Y, Kleinschmidt M, Hause G, Willbold D, Funke SA, Schilling S, Demuth HU (2009) Pyroglutamate formation influences solubility and amyloidogenicity of amyloid peptides. Biochemistry 48:7072–7078.

Schmitz C, Hof PR (2000) Recommendations for straightforward and rig-

orous methods of counting neurons based on a computer simulation approach. J Chem Neuroanat 20:93–114.

Selkoe DJ, Yamazaki T, Citron M, Podlisny MB, Koo EH, Teplow DB, Haass C (1996) The role of APP processing and trafficking pathways in the formation of amyloid beta-protein. Ann N Y Acad Sci 777:57–64.

Shankar GM, Li S, Mehta TH, Garcia-Munoz A, Shepardson NE, Smith I, Brett FM, Farrell MA, Rowan MJ, Lemere CA, Regan CM, Walsh DM, Sabatini BL, Selkoe DJ (2008) Amyloid-beta protein dimers isolated directly from Alzheimer's brains impair synaptic plasticity and memory. Nat Med 14:837–842.

Staufenbiel M, Paganetti PA (2000) Electrophoretic separation and immunoblotting of $A\beta 1-40$ and $A\beta 1-42$. Methods Mol Med 32:91–99.

Sturchler-Pierrat C, Abramowski D, Duke M, Wiederhold KH, Mistl C, Rothacher S, Ledermann B, Bürki K, Frey P, Paganetti PA, Waridel C, Calhoun ME, Jucker M, Probst A, Staufenbiel M, Sommer B (1997) Two amyloid precursor protein transgenic mouse models with Alzheimer disease-like pathology. Proc Natl Acad Sci U S A 94:13287–13292.

Takahashi RH, Milner TA, Li F, Nam EE, Edgar MA, Yamaguchi H, Beal MF, Xu H, Greengard P, Gouras GK (2002) Intraneuronal Alzheimer abeta42 accumulates in multivesicular bodies and is associated with synaptic pathology. Am J Pathol 161:1869–1879.

Thal DR, Sassin I, Schultz C, Haass C, Braak E, Braak H (1999) Fleecy amyloid deposits in the internal layers of the human entorhinal cortex are comprised of N-terminal truncated fragments of Abeta. J Neuropathol Exp Neurol 58:210–216.

Thal DR, Larionov S, Abramowski D, Wiederhold KH, Van Dooren T, Yamaguchi H, Haass C, Van Leuven F, Staufenbiel M, Capetillo-Zarate E (2007) Occurrence and co-localization of amyloid beta-protein and apolipoprotein E in perivascular drainage channels of wild-type and APP-transgenic mice. Neurobiol Aging 28:1221–1230.

Tomiyama T, Matsuyama S, Iso H, Umeda T, Takuma H, Ohnishi K, Ishibashi K, Teraoka R, Sakama N, Yamashita T, Nishitsuji K, Ito K, Shimada H, Lambert MP, Klein WL, Mori H (2010) A mouse model of amyloid β oligomers: their contribution to synaptic alteration, abnormal tau phosphorylation, glial activation, and neuronal loss *in vivo*. J Neurosci 30:4845–4856.

Wirths O, Breyhan H, Cynis H, Schilling S, Demuth HU, Bayer TA (2009) Intraneuronal pyroglutamate-Abeta 3–42 triggers neurodegeneration and lethal neurological deficits in a transgenic mouse model. Acta Neuropathol 118:487–496.

Yamaguchi H, Sugihara S, Ogawa A, Saido TC, Ihara Y (1998) Diffuse plaques associated with astroglial amyloid beta protein, possibly showing a disappearing stage of senile plaques. Acta Neuropathol 95:217–222.

Journal of Neurochemistry

JOURNAL OF NEUROCHEMISTRY | 2012 | 121 | 774–784 doi: 10.1111/j.1471-4159.2012.07707.x

ORIGINAL ARTICLE

N-Terminal pyroglutamate formation of Aβ38 and Aβ40 enforces oligomer formation and potency to disrupt hippocampal long-term potentiation

Dagmar Schlenzig,* Raik Rönicke,† Holger Cynis,* Hans-Henning Ludwig,* Eike Scheel,* Klaus Reymann,† Takaomi Saido,‡ Gerd Hause,§ Stephan Schilling* and Hans-Ulrich Demuth*

*Probiodrug AG, Halle/Saale, Germany

†Deutsches Zentrum für Neurodegenerative Erkrankungen, c/o Leibniz-Institut für Neurobiologie, Magdeburg, Germany

‡Laboratory of Proteolytic Neuroscience, RIKEN Brain Science Institute, Wako, Saitama, Japan

§Biozentrum der Martin-Luther-Universität, Halle/Saale, Germany

Abstract

Pyroglutamate (pGlu)-modified amyloid peptides have been identified in sporadic and familial forms of Alzheimer's disease (AD) and the inherited disorders familial British and Danish Dementia (FBD and FDD). In this study, we characterized the aggregation of amyloid-β protein Aβ37, Aβ38, Aβ40, Aβ42 and ADan species *in vitro*, which were modified by N-terminal pGlu (pGlu-Aβ3-x, pGlu-ADan) or possess the intact N-terminus (Aβ1-x, ADan). The pGlu-modification confers rapid formation of oligomers and short fibrillar aggregates. In accordance with these observations, the pGlu-modified Aβ38, Aβ40 and Aβ42 species inhibit hippocampal long term potentiation of synaptic response, but pGlu-Aβ3-42 showing the highest effect. Among the unmodified Aβ peptides, only Aβ1-42 exhibites such propensity, which was similar to pGlu-Aβ3-38 and pGlu-Aβ3-40. Likewise, the amyloidogenic peptide pGlu-ADan impaired synaptic potentiation more pronounced than N-terminal unmodified ADan. The results were validated using conditioned media from cultivated HEK293 cells, which express APP variants favoring the formation of Aβ1-x, Aβ3-x or N-truncated pGlu-Aβ3-x species. Hence, we show that the ability of different amyloid peptides to impair synaptic function apparently correlates to their potential to form oligomers as a common mechanism. The pGlu-modification is apparently mediating a higher surface hydrophobicity, as shown by 1-anilinonaphtalene-8-sulfonate fluorescence, which enforces potential to interfere with neuronal physiology.

Keywords: Aβ, ABri, ADan, Alzheimer's disease, amyloid, pyroglutamate.

J. Neurochem. (2012) **121**, 774–784.

ORIGINAL ARTICLE

The aggregation and deposition of various amyloid-β protein (Aβ) species in brain is a hallmark of Alzheimer's disease (AD). Aβ is released from amyloid precursor protein (APP) by consecutive cleavage of β-secretase and γ-secretase, generating the N- and C-terminus of Aβ, respectively. The proteolytic events result primarily in formation of Aβ1-40, to lower extent in Aβ1-42 and Aβ1-38. Accumulation of Aβ42 precedes that of Aβ40 but later on in AD progression Aβ40 becomes a significant species in deposits (Iwatsubo *et al.* 1994). Besides its well characterized C-terminal heterogeneity, also N-terminally modified Aβ peptides have been reported. Among those, species are generated which are modified at position 3 or 11 by pyroglutamic acid

Received October 6, 2011; revised manuscript received January 19, 2012; accepted February 16, 2012.

Address correspondence and reprint requests to Dr. Stephan Schilling, Probiodrug AG, Weinbergweg 22, 06120 Halle, Germany.
E-mail: stephan.schilling@probiodrug.de

Abbreviations used: Aβ, amyloid-β protein; ACSF, artificial cerebrospinal fluid; AD, Alzheimer's disease; ANS, 1-anilinonaphtalene-8-sulfonate; APP, amyloid-β precursor protein; fEPSP, excitatory post-synaptic field potential; FBD, familial British Dementia; FDD, familial Danish Dementia; HFIP, 1,1,1,3,3,3-hexafluoro-2-propanol; LTP, long-term potentiation; MES, 2-(N-morpholino)ethanesulfonic acid; MTA buffer, MES/Tris/acetate buffer; PAGE, polyacrylamide gel electrophoresis; PICUP, photo-induced cross-linking of unmodified peptides; Ru(Bpy), tris(2,2′-bipyridyl)dichlororuthenium(II); ThT, thioflavin T.

(pGlu). The deposition of N-terminally truncated and modified Aβ progresses during development of AD in contrast to normal aging. This has been shown for late onset sporadic AD as well as for familial AD cases associated with mutations in the presenilin 1 gene (Russo *et al.* 2000; Miravalle *et al.* 2005; Piccini *et al.* 2005; Güntert *et al.* 2006).

In previous studies, a prominent influence of the pGlu-modification on the pH-dependent solubility, aggregation propensity and fibril morphology of Aβ has been reported (Schilling *et al.* 2006; Schlenzig *et al.* 2009). Compared with full-length Aβ, solubility of pGlu-modified Aβ is reduced at physiological pH, which, in turn, increases the aggregation propensity. In contrast to Aβ1-40 fibrils, those of pGlu-modified Aβ40 are shorter and frequently arranged in bundles. A similar impact of the N-terminal pGlu modification was observed for the aggregation of the amyloid peptide ADan. ADan and ABri are the main components of amyloid deposits in hereditary FDD and FBD. These forms of dementia are very similar to AD with regard to brain histopathology. pGlu-modified amyloid accounts for the majority of the deposits in FDD and FBD (Ghiso *et al.* 2001). Also with ADan and ABri, we showed that the pGlu residue reduces the solubility and increases the aggregation propensity (Schlenzig *et al.* 2009).

Compelling evidence suggests a role of pre-fibrillar oligomers and potentially diffusible protofibrils in synaptotoxicity. To further address the influence of the N-terminus of Aβ and ADan on the oligomer formation and toxicity, we aimed at a characterization of the smaller aggregates and their impact on synaptic plasticity. The results should further clarify the potential role of N-terminal heterogeneity in amyloid peptides for the development and progression of different neurodegenerative disorders.

Materials and methods

Materials

Amyloid peptides were synthesized as described in the next section. All chemicals were of analytical grade.

Synthesis of amyloid peptides

Peptides were synthesized in 50 μmol scale on an automated Symphony synthesizer (Rainin) using Fmoc-strategy. Synthesis of ADan and pGlu-ADan was described previously (Schlenzig *et al.* 2009). Briefly, Fmoc-Tyr(tBu)-NovaSyn ®TGA resin (Merck KGaA, Darmstadt, Germany) was used as starting material. After deprotection and purification by RP-HPLC, the disulfide bond was introduced by iodine oxidation. Crude peptides were dissolved in AcOH/H_2O (4 : 1) to a final concentration of about 2 mg/mL. After addition of 10 equivalents of iodine the solution was stirred at 22°C for 1 h. Completion of the oxidation was followed by HPLC and MALDI-TOF mass spectrometry. The reaction was quenched by addition of water and the iodine was extracted with tetrachloromethane. The aqueous phase was lyophilized and purified on a 250 × 21 mm Luna C18 column (Phenomenex, Aschaffenburg, Germany) using a gradient of acetonitrile in water (0.04% trifluoroacetic acid).

For synthesis of Aβx-37, Aβx-38 and Aβx-40 the corresponding pre-loaded Fmoc-AA-NovaSyn ®TGA resins (Merck KGaA) were used. Gly-25 and Ser-26 were incorporated using the pseudoproline unit Fmoc-Gly-Ser($\psi^{Me,Me}$ Pro)-OH (Merck Biosciences). After deprotection, the crude peptides were purified on a 250 × 21 mm Luna C18 column using a gradient of acetonitrile in water (0.04% trifluoroacetic acid).

Aβx-42 was synthesized on Fmoc-Ala-NovaSyn ®TGA resin (Merck Biosciences). Gly-25 and Ser-26 were incorporated using isoacyl dipeptide Boc-Ser(Fmoc-Gly)-OH (4 eq.). It was coupled with HOBt (4 eq.)/N,N′-diisopropylcarbodiimid (4.4 eq.) for 2 × 45 min. The resulting 26-*O*-isoacyl-β-amyloid(x-42) was purified after deprotection by RP-HPLC. Subsequently, the depsipeptides were dissolved in 0.1 M ammonium bicarbonate (pH 7.4) for 1 h to initiate isoacyl conversion. The reaction was monitored by analytical RP-HPLC. Analytical HPLC analysis was performed on a 4.6 × 150 mm Source 5RPC column (5 μm; GE Healthcare, Bucks, GB) with a gradient made of solvent A (0.1% NH_4OH in H_2O at pH 9) and solvent B (acetonitrile/solvent A 60 : 40).

In case of all N-terminal pyroglutamated peptides the pGlu was incorporated as Boc-pGlu-OH.

ThioflavinT assay

The thioflavinT (ThT) assay was carried out as described previously (Schlenzig *et al.* 2009). Briefly, all peptides were disaggregated in 1,1,1,3,3,3-hexafluoro-2-propanol (HFIP; Sigma, St Louis, MO, USA) and their concentration was determined spectrophotometrically. HFIP was evaporated and peptides were dissolved in 0.1 M NaOH. The peptides were diluted using a three-buffer system consisting of 2-(N-morpholino)ethanesulfonic acid (MES)/Tris/acetate, 50/100/50 mM, pH 8.0 according to Ellis and Morrison (1982). The buffer provides a constant ionic strength over a broad pH range. If required, the pH was adjusted using 0.1 M HCl. The peptide solution was diluted 2 : 1 using 40 μM ThT in water (final ThT concentration 20 μM, containing 0.05% sodium azide). The peptide concentration in the assay (200 μL) was 25 μM of Aβ37, Aβ38 and Aβ40 species. Aβ42 species, ADan and pGlu-ADan were applied in concentrations of 5 μM. Only samples of Aβ42 contained 5% HFIP. The plate was covered by an adhesive film, incubated in a plate reader at 37°C and the ThT fluorescence recorded for up to 2 weeks (excitation 440 nm, emission 490 nm). For each peptide, measurements were performed in six cavities of one plate. Data were normalized using GraphPad Prism 4 Software. The first value in each data set was defined 0% and the largest value was defined 100%.

Photo-induced cross-linking of unmodified peptides

Photo-induced cross-linking of unmodified peptides (PICUP) chemistry was performed, essentially as described by Bitan *et al.* (2003). Here, a freshly dissolved 50 μM peptide solution in 10 mM sodium phosphate buffer (pH 7.5) was incubated for 30 min at 22°C. Afterwards, 36 μL were substituted with 2 μL of 1 mM Ru(Bpy) and 2 μL 20 mM of ammonium persulfate, both in 10 mM phosphate buffer. The cross-linking was initiated by a beam of visible light for 2 s and quenched by the addition of 40 μL 2-fold reducing sample

buffer (Invitrogen, Carlsbad, CA, USA). Samples were analyzed by sodium dodecyl sulfate–polyacrylamide gel electrophoresis (PAGE) using a 10–20% Tris–Tricine gel (Invitrogen) followed by silver staining (Pierce, Rockford, IL, USA).

Transmission electron microscopy

Samples were taken from freshly dissolved peptides and applied to Formvar-coated copper grids (Plano GmbH, Wetzlar, Germany), incubated for 60 s, washed three times with water and subjected to negative staining using 1% uranyl acetate. Images were taken with an EM 900 (Carl Zeiss SMT, Oberkochen, Germany) operating at 80 kV using a Variospeed SSCCD camera SM-1k-120 (TRS, Moorenweis, Germany).

Measurement of ANS fluorescence

Fluorescence of 1-anilinonaphtalene 8-sulfonate (ANS, 200 μM) in MES/Tris/acetate buffer (25/50/25 mM, pH 8.0) added to Aβ species (25 μM) was measured after an incubation time of 40 min at 37°C. Excitation was 350 nm and emission was scanned from 400 to 650 nm on a Fluorimeter LS 50 B (Perkin Elmer, Waltham, MA, USA).

Long-term potentiation

For measuring the influence of various Aβ species, ADan and pGlu-ADan on long-term potentiation (LTP) acutely isolated hippocampal slices (400 μm thickness) were prepared from 4-month-old male C57Bl/6 mice (breeding stock of the Leibniz Institute for Neurobiology) as described previously (Rönicke *et al.* 2011). After decapitation both hippocampi were isolated and transverse hippocampal slices were prepared using a tissue chopper with a cooled stage. The slices were maintained in a pre-chamber containing 8 mL permanently carbogen-gasified artificial CSF (ACSF, 124 mM NaCl, 25.6 mM $NaHCO_3$, 1.2 mM KH_2PO_4, 4.9 mM KCl, 2.5 mM $CaCl_2$, 2 mM $MgSO_4$, 10 mM glucose) to allow peptide or the respective solvent control application for 2 h. HFIP-treated peptides (as described for the ThT assay) were dissolved in dimethylsulfoxide (Sigma) to a concentration of 50 μM, sonicated and immediately added to the ACSF containing pre-chamber at final concentrations of 500 or 250 nM. After treatment with peptides, the slices were transferred into a submerged-type recording chamber, where they recovered for at least 30 min before starting with the electrophysiological experiments. The recording chamber was constantly perfused with ACSF at a rate of 2.5 mL/min at 33 ± 1°C. Synaptic responses were elicited by stimulation of the Schaffer collateral–commissural fibers in the stratum radiatum (CA1 region) by using lacquer coated stimulating electrodes of stainless steel. Field excitatory post-synaptic potentials (fEPSP) were recorded with glass electrodes (filled with ACSF, 14 MΩ) that were placed in the apical dendritic layer. The initial slope of the fEPSP was used as measure of this potential. The stimulus strength of the test pulses was adjusted to 30% of the fEPSP slope maximum. During baseline recording single stimuli were applied every minute. Once a stable baseline had been established, long-term potentiation was induced by applying three series of strong tetanus pulses. The interval between the three series was 10 min. Each series consisted of hundred 0.2 ms pulses at 10-ms intervals.

For measuring the influence of Aβ-conditioned medium on LTP, acute isolated slices from rats were prepared basically as described (Rönicke *et al.* 2009). Seven- to 8-week-old male Wistar rats (Harlan Laboratories, Borchen, Germany) were decapitated, their brains quickly removed and placed into ice-cold ACSF having the same composition as described above. Both hippocampi were isolated and transverse hippocampal slices (400 μM thickness) were prepared. The slices were maintained in a pre-chamber containing 8 mL permanently carbogen-gasified Aβ-conditioned medium (total Aβ 3 ng/mL, approximately 700 nM) or control medium for 2 h. Then, slices were placed into an interface recording chamber and were allowed to recover for at least 1 h. The chamber was constantly perfused with Ringer solution at a rate of 1 mL/min. The surface of the slices was exposed to a moist carbogen atmosphere, which was exchanged at a rate of 20 L/h. The temperature of the chamber was maintained at 34 ± 1°C. Synaptic responses were elicited by stimulation of the Schaffer collateral–commissural fibers in the stratum radiatum (CA1 region) basically as described above, but during baseline recording three single stimuli (10-s interval) were averaged every 5 min.

Preparation and analysis of conditioned media

Human embryonic kidney cells (HEK293) were cultured in Dulbecco's modified eagle medium supplemented with 10% fetal bovine serum and Gentamycin in a humidified atmosphere of 5% CO_2 at 37°C. Cells were seeded into 75 cm^2 flasks and transfected the next day with vectors APP-NL, APP-NLE, APP-NLQ (Shirotani *et al.* 2002; Cynis *et al.* 2008) and pcDNA3.1 for control using Lipofectamin2000 (Invitrogen) according to the manufacturer's guidelines. The medium was exchanged with Dulbecco's modified eagle medium without phenol red, fetal bovine serum and Gentamycin 24 h later. After additional 20 h the supernatant was collected and centrifuged at 1 000 *g* for 5 min to remove remaining cells. Samples were taken for Aβ ELISA, immunoprecipitation and size exclusion chromatography (SEC) and the remaining medium was readily frozen at −80°C until use. Before incubating the slices, Aβ concentration was determined by specific sandwich ELISA detecting total Aβx-40 (IBL-International, Hamburg, Germany) and normalized to 3 ng/mL by the addition of conditioned medium. After immunoprecipitation, the Aβ composition was analyzed using western blot, applying 15% urea–PAGE gels according to Klafki *et al.* (1996).

To investigate the oligomeric state of Aβ, conditioned media were centrifuged to remove insoluble material at 13 000 *g* for 15 min and subjected to size exclusion chromatography on a Superdex 75 10/300 column (GE Healthcare, Bucks, GB). The mobile phase consisted of 50 mM Tris, 100 mM NaCl, pH 8.0. 250 μL were injected, fractions of 1 mL collected and the concentration of Aβ determined by ELISA.

Results

Fibril formation of Aβ and ADan peptides

In our previous investigations, we characterized the formation of fibrils from N-truncated and pGlu-modified Aβ40 peptides (Schilling *et al.* 2006; Schlenzig *et al.* 2009). In these studies, the peptides exhibited enhanced aggregation propensity due to truncation and modification of their N-termini. Here, we aimed at a characterization of the role of the pGlu-modification for the aggregation propensity of other C-terminal

variants of Aβ, that is, Aβ37, Aβ38 and Aβ42. The isoelectric point of the peptides and thus the pH value has been shown to exert a significant influence on the solubility of peptides, as shown previously for Aβ40. Because a C-terminal truncation does not change the theoretical pI of the Aβ variants (Aβ1-37/38/40/42 pI = 5.43; pGlu-Aβ3-37/38/40/42 pI = 6.62; ADan pI = 6.49; pGlu-ADan pI = 6.95; pI calculated with peptide property calculator from GenScript, using an acetylated amino acid to mimic pGlu; https://www.genscript.com/ssl-bin/site2/peptide_calculation.cgi), we characterized the aggregation of the peptides at pH 8.0, a pH which is fairly distant from the pI of all amyloid peptides analyzed.

The fibril formation from Aβ1-40 required a long lag time of about 150–200 h, that of Aβ3-40 even longer (about 400 h, Figure S1a). In contrast, as observed previously the incubation of monomeric pGlu-Aβ3-40 caused a significantly accelerated aggregation (Fig. 1a). Interestingly, a C-terminal truncation by two amino acids did not reduce the aggregation propensity. The characteristic exponential fibril growth was observed with Aβ1-38 after about 100 h incubation time (Fig. 1b). Again, the N-terminal pGlu-modification decreased the lag phase. Furthermore, C-terminal truncation resulting in Aβx-37 did not have a significant effect on aggregation propensity, but similar to the other Aβ species, pGlu-Aβ3-37 aggregated faster than Aβ1-37 (Fig. 1c). A decline of the ThT signal was observed with pGlu-Aβ3-40 and pGlu-Aβ3-37 at the end of the period of investigation. Such a phenomenon was previously attributed to formation of higher ordered, suprafibrillar assemblies (Walsh *et al.* 2001). The electron microscopic images indeed support different morphologies of pGlu-Aβ and Aβ1-x fibrils. We found mainly smooth fibrils in case of Aβ1-x but shorter fibrils that strongly tend to form lateral interactions for pGlu-Aβ3-x species (images are displayed in Fig. 1).

In contrast to the C-terminally truncated peptides, both Aβ42-derivatives displayed fibril formation within a few hours. As the rapid formation did not allow a reliable observation of a lag-phase (Figure S1b), we added 5% HFIP to tune down the β-sheet formation to both reactions. Although the relative difference in the lag phase was not as substantial as for the C-terminally truncated peptides, pGlu-Aβ3-42 showed again accelerated fibril formation (Fig. 1d).

Finally, we characterized the *in vitro* fibril formation of ADan and pGlu-ADan (Fig. 1e). An exponential increase of fluorescence intensity was observed with pGlu-ADan. In contrast, we did not observe a significant change of fluorescence intensity with ADan under these conditions, implying slow aggregation. Only few fibrils could be found after 10 days of incubation.

Thus, the formation of larger aggregates of all peptides is influenced by the N-terminal amino acid in a similar manner, although the degree of acceleration by N-terminal pGlu differs between the amyloid species.

Oligomer formation – PICUP

As the assembly of amyloid peptides into fibrillar aggregates, which are detected by ThT-fluorescence, represents a seeded process, we aimed at a characterization of the formation of oligomers. To investigate potential differences we applied PICUP. PICUP enables visualization of small oligomers like dimers, trimers and tetramers that are usually unstable in sodium dodecyl sulfate–PAGE (Bitan *et al.* 2003). Using the method, two populations of oligomers are obtained. One population is due to stochastic formation controlled by diffusion processes and one is caused by cross-linking of preformed oligomers that are in a dynamic equilibrium within the incubation solution. To investigate the early events during the aggregation process, the cross-linking was performed directly after dissolution of the monomeric peptides.

Applying PICUP to various Aβ species, we obtained a similar pattern of oligomer ladders with Aβ1-37, Aβ1-38 and Aβ1-40 with a slightly pronounced band corresponding to trimers (Fig. 2a; first lanes). The respective N-terminally truncated Aβ3-x species showed a very similar pattern (Figure S2). For pGlu-Aβ3-37, pGlu-Aβ3-38 and pGlu-Aβ3-40, however, remarkable differences could be observed. Here, the band of trimers is pronounced and significantly broadened (Fig. 2a, second lanes). Such an oligomeric pattern was also observed, if low molecular weight fractions of Aβ after size-exclusion chromatography were applied to cross-linking, as exemplarily shown for Aβ1-40 and pGlu-Aβ3-40 in Fig. 2c. Thus, the oligomers were not preformed, but rather rapidly generated in aqueous solution. In contrast to Aβ1-37/38/40, PICUP analysis of Aβ1-42 and pGlu-Aβ3-42 revealed a significant fixation of trimers and tetramers (Fig. 2a). A densitometric analysis highlights the intense bands of pGlu-Aβ3-x trimers/tetramers, which appears similar to Aβ1-42/pGlu-Aβ3-42 (Fig. 2b).

The cross-linking of ADan and in particular of pGlu-ADan led to fixation of oligomers with higher molecular weight. Both peptides apparently formed pentamers/hexamers. However, the bands are more intense with pGlu-ADan than with ADan, which appeared diffuse (Fig. 2a). In addition, we observed a strong signal for large oligomeric forms of pGlu-ADan. These higher aggregates hardly entered the separation gel.

Transmission electron microscopic analysis of oligomers

To further substantiate the differences observed in PICUP analysis, we assessed Aβ38, Aβ40, Aβ42 and ADan in electron microscopy. Comparing the electron micrographs of freshly dissolved Aβ1-38/40 and pGlu-Aβ3-38/40, clear differences are observed depending on the N-terminus of the peptides (Fig. 3). Aβ1-38 and Aβ1-40 form very small structures (Fig. 3a and c) whereas pGlu-Aβ3-38 and pGlu-Aβ3-40 form larger conglomerates (Fig. 3a and d). Similarly, rather globular aggregates were observed with pGlu-Aβ3-42 (Fig. 3f). In contrast, early oligomers of Aβ1-42 have a more wormlike appearance (Fig. 3e). Thus, although the size of

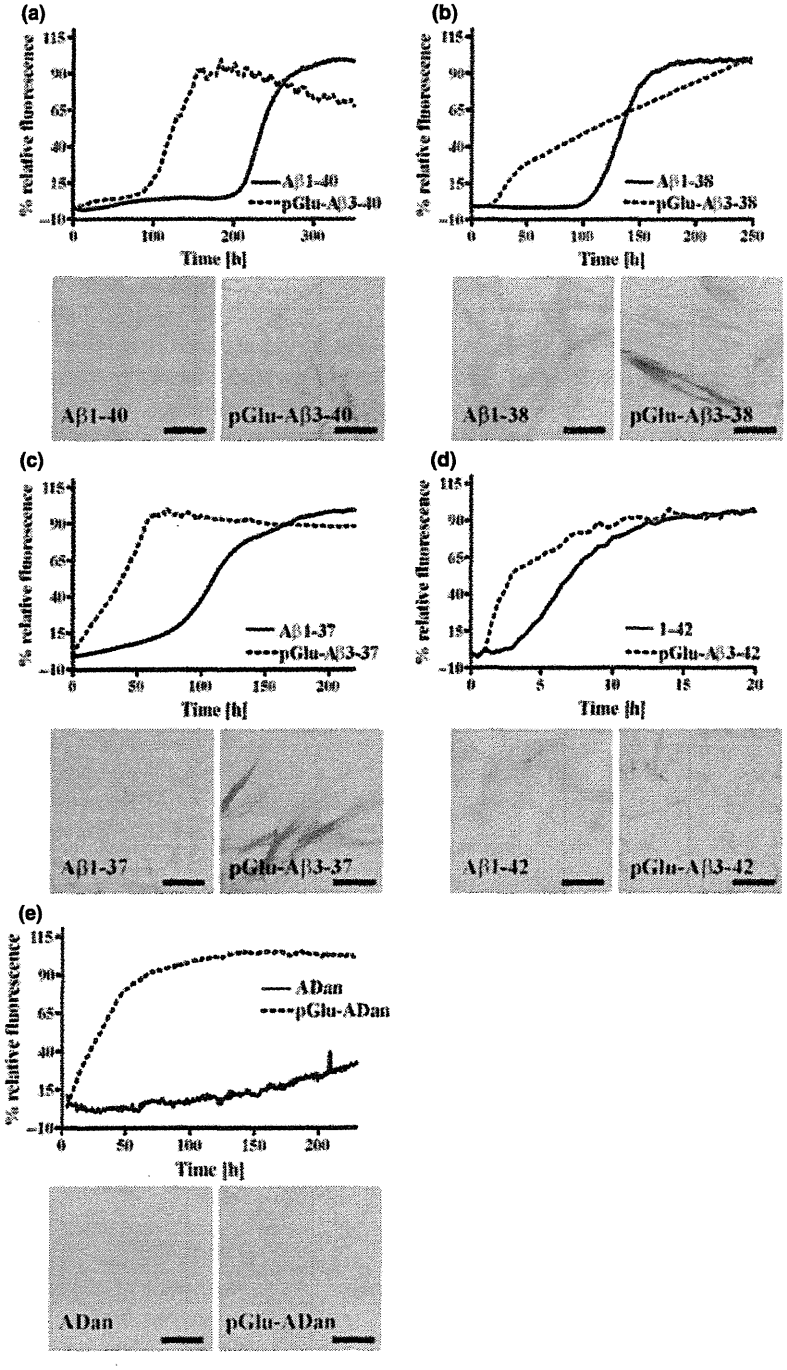

Fig. 1 Aggregation kinetics of different Aβ and ADan species, monitored by ThT-fluorescence. The diagrams correspond to: Aβ40 (a), Aβ38 (b), Aβ37 (c), Aβ42 (d) and ADan (e). In addition, electron micrographs of the fibrillar aggregates are provided. The concentration of Aβ40, Aβ38 and Aβ37 was 25 μM, whereas the concentration of Aβ42 and ADan was 5 μM (ThT 10 μM, 0.05% sodium azide). Samples of Aβ42 contained 5% HFIP. Measurements were performed as 6 replicates and data were normalized to 100%. All reactions were carried out at pH 8.0 and 37°C. Bars in micrographs indicate 200 nm; magnification was 50 000×. For all amyloid peptides investigated, the N-terminal pGlu-modification leads to an acceleration of aggregation compared with non-modified peptides. Furthermore, fibrils of pGlu-modified amyloid peptides are shorter and strongly tend to form lateral interactions.

the oligomers is not reliably obtained by our transmission electron microscopic analysis, substantial differences between Aβ peptides are also observed without chemical cross-linking, further supporting rapid aggregation if the N-terminus is truncated and pGlu-modified.

The shape of the oligomeric forms of ADan and pGlu-ADan was rather similar to each other (Fig. 3g and h). The main difference appeared to be that the pGlu-peptide formed aggregates of larger size, which mirrors the observations from the PICUP analysis.

Analysis of ANS fluorescence

To compare the apolar nature of unmodified versus pGlu-modified Aβ, changes in fluorescence of ANS as a measure of surface hydrophobicity (Cardamone and Puri 1992) was investigated. In general, the ANS fluorescence intensity is

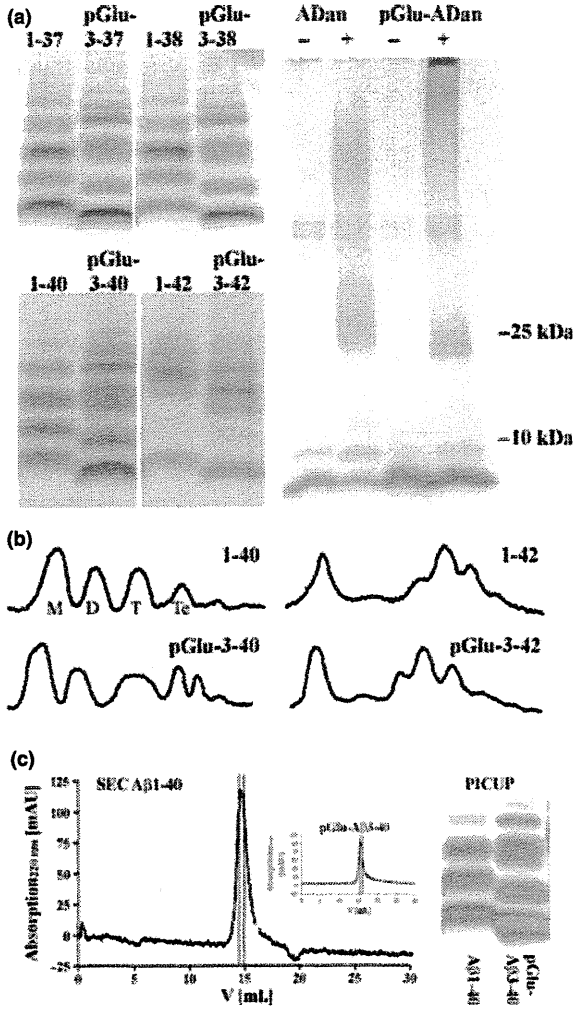

Fig. 2 (a) SDS–PAGE analysis of Aβ37, Aβ38, Aβ40, Aβ42 and ADan following photo-induced cross-linking of the unmodified peptides (PICUP). For Aβ, the first lane in each picture corresponds to the full-length species (Aβ1-x), whereas the second lane contains the respective pGlu-modified peptide (pGlu-Aβ3-x). In case of ADan, non-cross-linked (–) and cross-linked (+) peptide preparations are compared. A densitometric analysis of the band pattern of Aβ40 and Aβ42 is provided in panel (b); (M-monomer, D-dimer, T-trimer, Te-tetramer). The results of the PICUP analysis did not differ if Aβ was separated by size exclusion chromatography prior to cross-linking, as shown for Aβ1-40 and pGlu-Aβ3-40 (c). All products were analyzed by 10–20% Tris–Tricine gel electrophoresis and visualized by silver staining. The pGlu-modification significantly enforces the formation of small oligomers from Aβ37, Aβ38 and Aβ40. The effect is not obvious with Aβ42. Differences are also observed with pGlu-ADan, although these aggregates appear much larger compared with the Aβ oligomers detected.

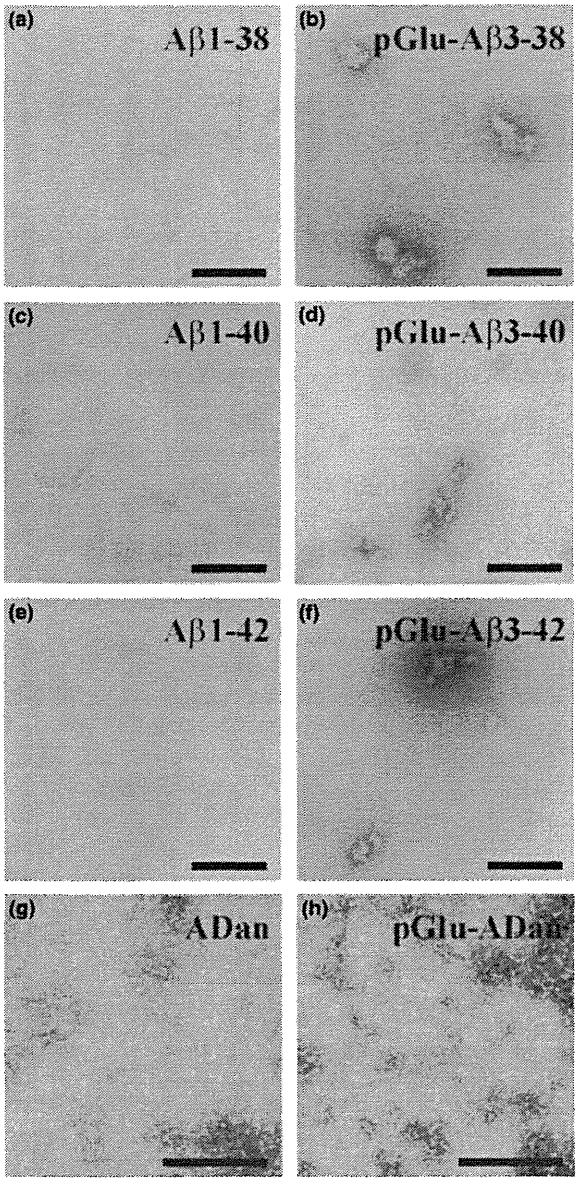

Fig. 3 Electron micrographs of small aggregates of amyloid peptides Aβ1-38 (a), pGlu-Aβ3-38 (b), Aβ1-40 (c), pGlu-Aβ3-40 (d), Aβ1-42 (e), pGlu-Aβ3-42 (f), ADan (g) and pGlu-ADan (h). Aβ38, Aβ40 (25 μM) and Aβ42 (5 μM) were dissolved in 10 mM sodium phosphate buffer, pH 7.5 and incubated for 30 min. ADan peptides (25 μM) were dissolved in MTA-buffer pH 4.0. In contrast to N-terminally unmodified Aβ, the pGlu-modified Aβ species form larger, globular oligomeric aggregates. ADan and pGlu-ADan associate into worm-like aggregates, which appear larger for the pGlu-modified peptide species, supporting the observations from PICUP analysis. Bars in micrographs indicate 200 nm; magnification was 50 000× or 85 000×.

lower in the presence of C-terminally truncated Aβx-40 compared with Aβx-42 (Fig. 4). In particular, freshly dissolved Aβ1-40 and Aβ3-40 (Figure S3) do not have any effect on ANS fluorescence. The pGlu-modified Aβ shows a significantly stronger influence on the fluorescence intensity of ANS and results in a shift of maximum emission from 519

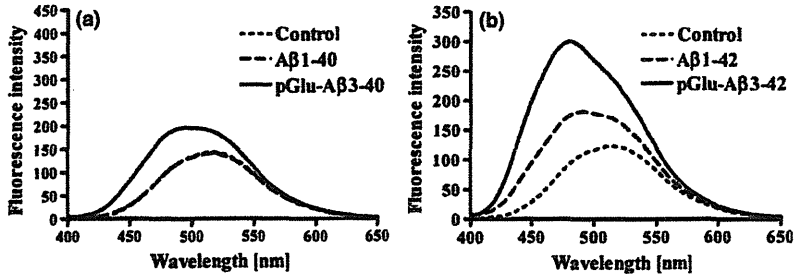

Fig. 4 Influence of Aβ on fluorescence intensity of ANS. Peptide concentration was 25 μM in MES/Tris/acetate buffer pH 8.0, 200 μM ANS. Peptides were incubated at 37°C for 40 min prior to measurement. pGlu-Aβ3-40 has an increasing influence on fluorescence intensity of ANS, whereas fluorescence curves of control and Aβ1-40 appear identical (a). Aβ1-42 and pGlu-Aβ3-42 increase fluorescence intensity of ANS. Compared with Aβ1-42, pGlu-Aβ3-42 triggered a fluorescence increase which appeared twofold stronger and further blue-shifted (b).

to 480 nm, suggesting a fast formation of aggregates with a more hydrophobic surface.

Influence of synthetic Aβ and ADan on hippocampal LTP

To address the functional consequences of the different oligomers formed from Aβ and ADan and their truncated and pGlu-modified counterparts, we assessed the influence of the Aβ38, Aβ40, Aβ42 and ADan peptides on long-term potentiation of synaptic response in hippocampal slices from mice. Here, freshly dissolved Aβ1-38, Aβ1-40 (Fig. 5a and c) and Aβ3-40 (Figure S4) did not show any effect on synaptic function at a concentration of 500 nM. In contrast, pGlu-Aβ3-38 and pGlu-Aβ3-40 both significantly impaired the LTP at that concentration (Fig. 5b and d). Thus, apparently, the accelerated aggregation mediated by the N-terminus (compare Figs 1 and 2) leads to a rapid generation of ANS fluorescence effecting oligomers which impair the neuronal function.

In accordance with this interpretation, Aβ1-42 and pGlu-Aβ3-42 impaired hippocampal LTP (Fig. 6a and b, insets) at a concentration of 500 nM. A lower Aβ concentration revealed a higher activity of pGlu-Aβ3-42 to affect potentiation. Thus, the N-terminus of Aβ42 clearly influences the synaptotoxic potential at lower concentration.

Finally, we also assessed the influence of the amyloidogenic peptides ADan and pGlu-ADan on hippocampal LTP. Interestingly, pGlu-ADan impaired the potentiation in a similar concentration as the Aβ peptides applied at 500 nM. However, the reduction in LTP caused by the non-modified ADan peptide did not reach statistical significance (Fig. 6c and d).

Influence of cell-born Aβ on hippocampal LTP

To substantiate the findings obtained with synthetic Aβ we collected conditioned media from HEK293 cells which secrete primarily Aβ1-40, Aβ3-40 or pGlu-Aβ3-40

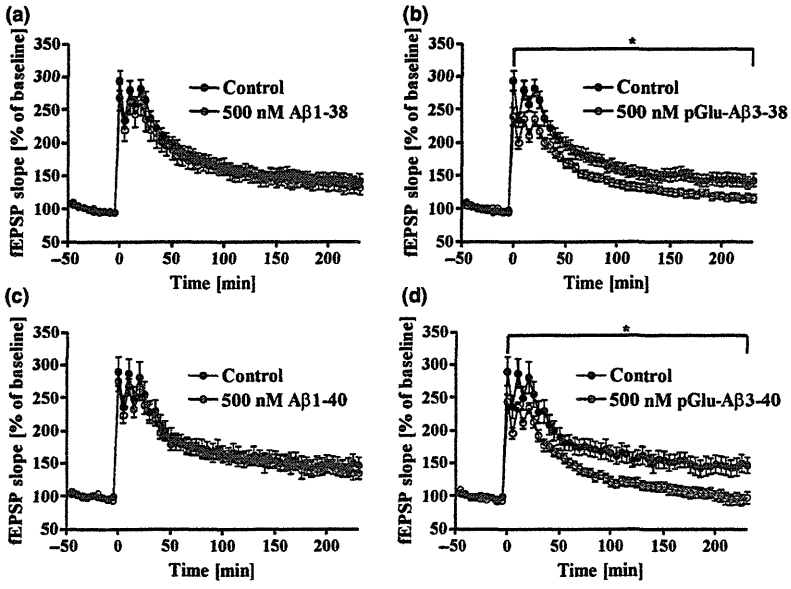

Fig. 5 Influence of freshly dissolved Aβ1-38 (a), pGlu-Aβ3-38 (b), Aβ1-40 (c) and pGlu-Aβ3-40 (d) on long-term potentiation (LTP) in acute hippocampal slices from mice. The amyloid peptides were dissolved in DMSO and diluted in ACSF to a final concentration of 500 nM, controls did not contain the peptide. In accordance with the observation of oligomers, only pGlu-Aβ3-38 and pGlu-Aβ3-40 impaired the neuronal physiology. For experimental details, see Methods (control: $n \geq 17$, peptide: $n \geq 12$, $^*p \leq 0.05$ ANOVA with repeated measures).